Nazca Mummies. CT Scan Analysis.

Galetskii D. BV, m.d., PhD.

Associate Professor of the Department of Dentistry, Surgical and Maxillofacial Surgery, First Saint Petersburg Medical University named after Academician I.P. Pavlov, Saint Petersburg, Russia.

A detailed analysis of CT scans of two unique mummies discovered in the caves of the Nazca region is presented. To facilitate comprehension, analogous scans are positioned on opposing sides of the book spread. The material is intended for all interested specialists and enthusiasts who are interested in a more detailed understanding of this unique phenomenon.

Contents

Introduction

In 2017, in the Nazca region of Peru, a local resident made a remarkable discovery: strange three-fingered mummies in mountain caves. The local resident subsequently contacted Jaime Moussan, a Mexican journalist, who in turn contacted the American company Gaia. Gaia proceeded to organise an expedition for the purpose of examining the mummies. A comprehensive account of this episode can be found in the book "The Mysterious Mummies of Nazca" by K. G. Korotkov, published by Stigmalion in 2019. This book presents the results of DNA analysis, chemical composition of tissues and CT tomography of the mummy named Maria. The DNA analysis of Maria revealed her classification as Homo sapiens; however, a lack of genetic similarity was identified between Maria and any known human population. The age of the mummy was determined to be approximately 1800 years. This period corresponds to the heyday of the Nazca culture. However, it is important to note that during this period, humans were not able to plan for the future due to their reliance on the unpredictability of natural phenomena.

In 2025, we received CT scans of another mummy from Peru, courtesy of our colleagues in Peru. This mummy was named Montserrat. The specimen was of particular interest due to the presence of a foetus beneath her heart. The cranium of Montserrat's specimen exhibited a distinctive elongation, a trait that has been observed in numerous other specimens of similar species, including those unearthed in Crimea and at Stonehenge. A significant collection of such skulls is exhibited in the Paracas Museum in Peru. This paper presents a comparative analysis of CT scans of both mummies, providing detailed information on each.

The study of mummies is of considerable historical and archaeological significance. The preservation of the mummies enables detailed examination and comprehensive study. Mummified organs, preserved in excellent condition (unlike Egyptian mummies, where the organs were removed after death),

allow us to gain insight not only into the anatomy and diseases of these creatures, but also, if desired, after rehydration, to learn the microstructure of the tissues and conduct DNA analysis. However, it is imperative to acknowledge that the process of mummification entails certain alterations associated with tissue dehydration, resulting in changes to the size of the hollow organs. The examination of these bodies is akin to delving into the annals of centuries past. Through meticulous inspection and analysis, we gain insight into the final moments of these creatures' lives. The authors facilitate the reader's ability to comprehend the harrowing narrative by providing a comprehensive overview of the injuries that ultimately resulted in death.

Given the plethora of conclusions arrived at by so-called "armchair experts" regarding the presence of what are termed "obvious fakes", it is important to acknowledge that these creatures possess anatomical features that defy facile assembly akin to a construction set. In the present study, an attempt was made to conduct a detailed analysis of the skin and to describe the violations of its integrity as thoroughly as possible. We are unable to definitively ascertain whether the presence of three fingers is an obvious indication of a fake, nor can we rule out this possibility. One hypothesis could be that the presence of three fingers is indicative of a genetic experiment by nature, or perhaps the presence of a separate species of living creatures. To address these inquiries, a comprehensive biochemical examination of the tissues and a histological study are imperative. In this book, we have organised the text and images so that the reader can select their preferred method of reading: either reading, immediately comparing the anatomical features, or choosing the path to read about each of the mummies in full, and then compare them themselves.

Body position

Maria

Initially, it was hypothesised that this creature was female, although a detailed analysis did not reveal any signs characterising gender, and the pelvic organs were absent. The estimated age of Maria is 35-45 years, as indicated by the condition of the teeth and skeletal bones. The body of Maria is of regular build. Her height is estimated to be approximately 168 cm. The arms are flexed at an angle of approximately 60 degrees at the elbow joint, with the fingers of both hands clasping the opposite shoulder in the upper third. The forearms are positioned in a crossed configuration over the thorax, thereby fixing the knees. The legs are flexed at the knee joint at an angle of approximately 22 degrees. The distance between the feet in the heel area is measured at 76 mm.

Postmortem changes indicate that Maria was most likely positioned on her right side upon death. This is indicated by the direction of the hanging folds of skin and the tilt of the head, which is tilted and turned to the right, and the right parietal bone is pressed to the ground.

Monserrat

This is a woman whose presumed age is 16-25 years, as indicated by the condition of the dental and jaw system and skeletal bones. In addition, she is clearly pregnant. Montserrat's height is approximately 160 cm.

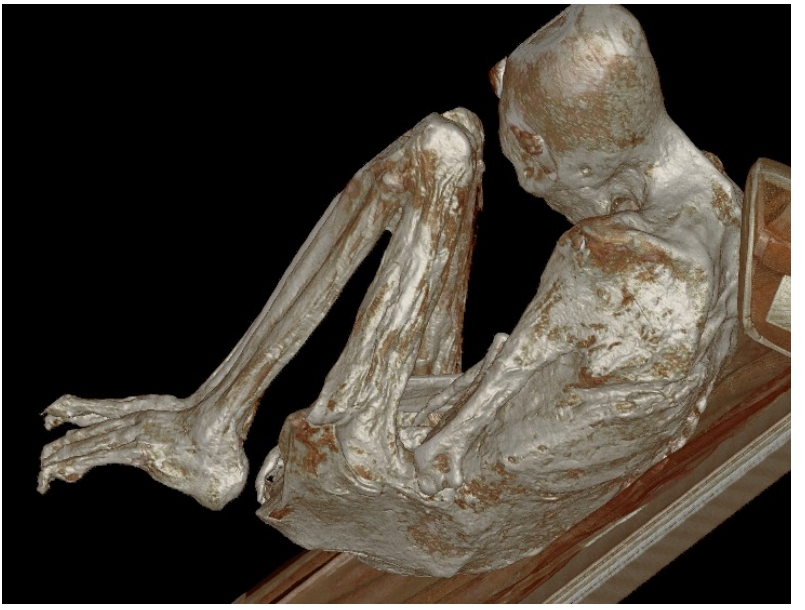

The left arm is flexed at a 37-degree angle at the elbow joint, maintaining this position whilst positioned on the anterior aspect of the pregnant woman's abdomen. The right arm is positioned at a 94-degree angle, with the fingers extending to the perineum area. The knees are flexed at a joint angle of approximately 38 degrees on the right and 33 degrees on the left. The distance between the feet in the heel area is 25 mm.

Maria

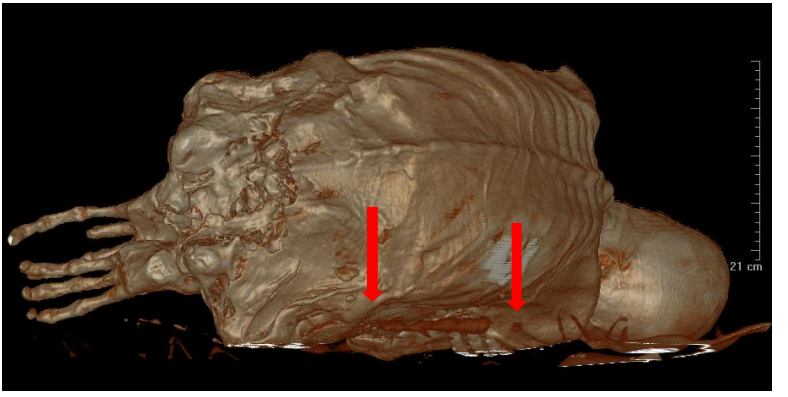

The direction of the folds in the skin indicates a specific orientation.

Upon thorough examination, a conspicuous laceration, accompanied by signs of biting or contusion, was identified in the region of the small pelvis. In addition, numerous linear and punctate lacerations were observed, presumably resulting from claw injuries or a fall onto stone surfaces. These lacerations extend from the coccyx to the hip joint. The skin and subcutaneous fat have been removed, and two vertebrae of the coccygeal region are broken off.

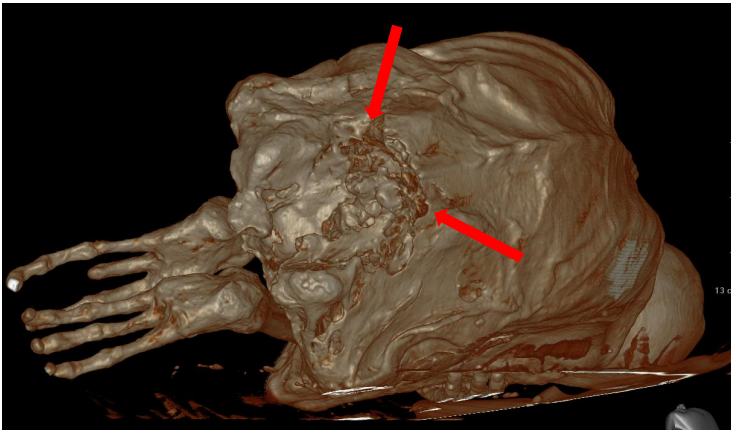

Trace of a suspected bite.

Monserrat

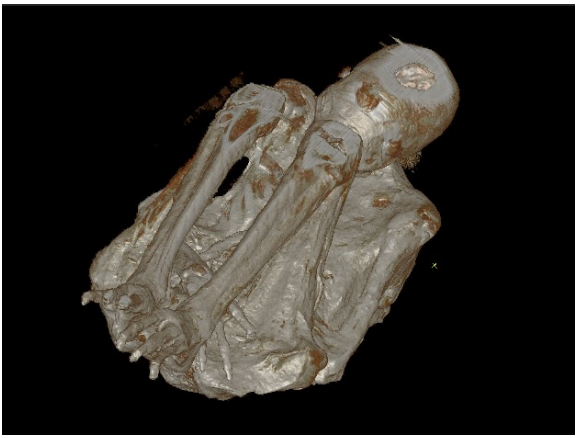

Position at the mumification.

It is reasonable to hypothesise that the cause of death was a significant degree of trauma sustained over an extended period. The integrity of the skin at the front of the right chest, between the fifth and sixth ribs, was compromised, and this finding is consistent with the characteristics of a puncture wound.

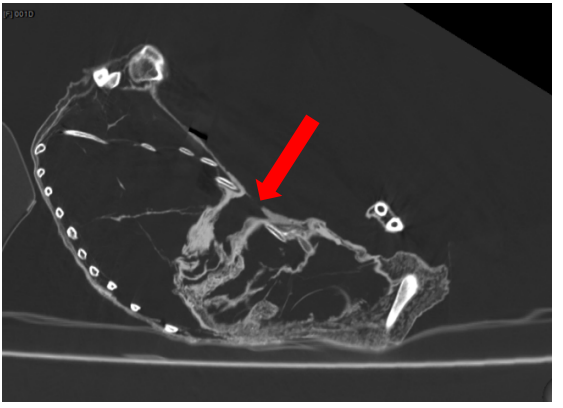

CT scan - oblique sagittal plane, passes through the wound channel (shown by the arrow).

Maria

Skin defect boundaries (CT screen sagittal plane).

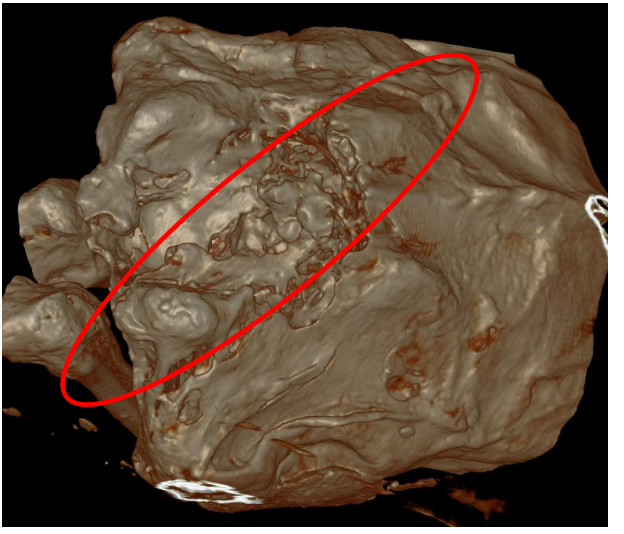

This is indicative of an injury sustained by a non-sharp object, such as a claw or a fall onto rocks. The wound exhibits a zigzag shape and broken line, indicative of damage to the skin of the buttock, accompanied by the formation of skin folds. The wound's edges are uneven and jagged.

Monserrat

When examining the liver, it is also evident that at the site of tissue rupture, due to dehydration, the edges of the wound channel have diverged over a significant distance.

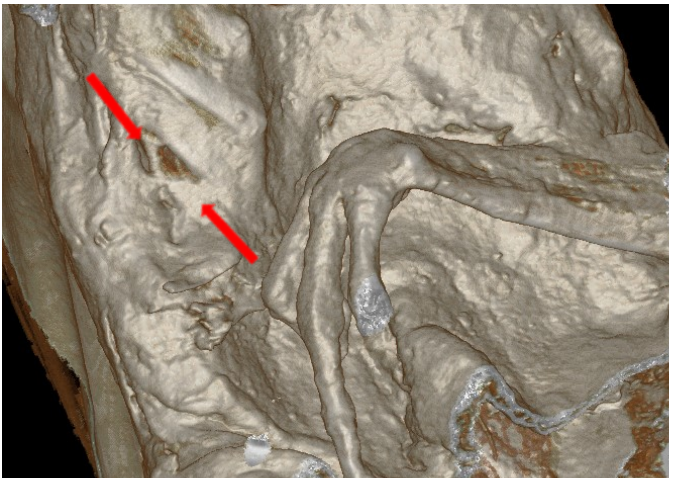

Chest wound. CT reconstruction.

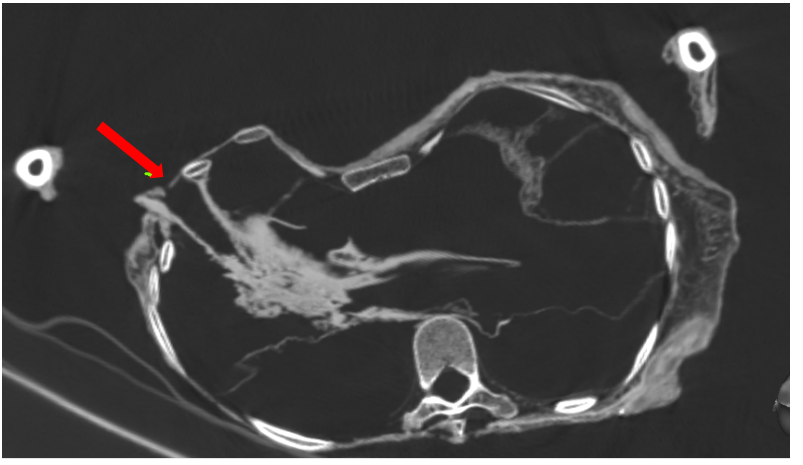

A CT scan reveals a horizontal plane that passes through the wound channel (illustrated by the arrow). It is evident that there has been a rupture of liver tissue at the level of the skin injury, directly with the site of the stab wound.

Maria

A mark resulting from injury by a non-sharp object (possibly a claw or falling on rocks) is described. The injury manifests as a zigzag shape and a broken line of the wound, characterised by the formation of skin folds. Multiple lesions are visible, indicating that a significant fragment of tissue was torn off, and that foreign bodies penetrated the bone joints, the oral cavity, and the area behind the eyelid.

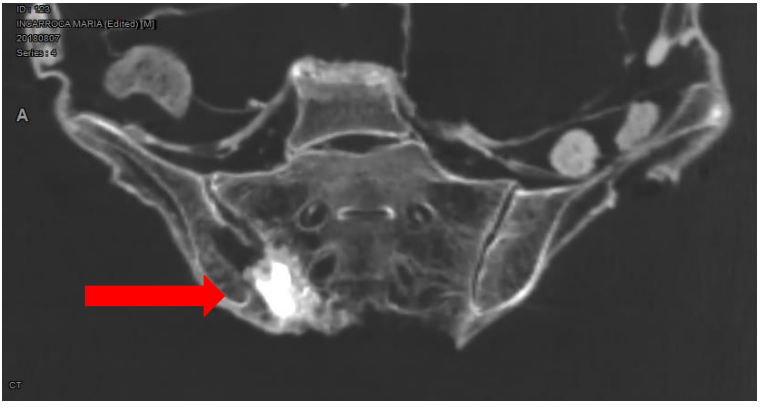

A foreign body in the lumbosacral joint (frontal plane).

In the event that the hypothesis of a bite mark is to be considered, the distance between the fangs is measured at 57 mm, with the fang mark located on the same plane as the central teeth. This may be indicative of an animal belonging to the feline family, such as a puma (it should be noted that among representatives of the dog family, the fangs are not located on the same line as the incisors). It is a well-documented fact that pumas were once widespread in the Peruvian mountains and were known to attack humans.

Monserrat

Upon her demise, it is probable that she was in a vertical position, with her back in contact with a rigid surface. While the majority of the folds are oriented in a downward direction (green arrows), those located on the posterior are directed in an upward direction (red arrows). Additionally, a trace of a flat surface is discernible on the left buttock.

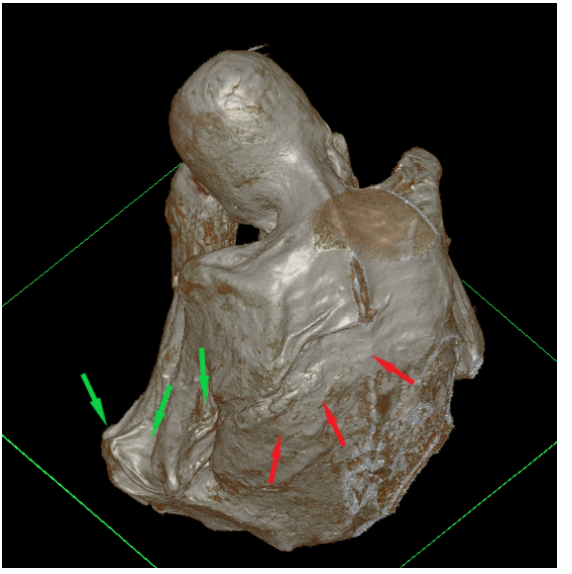

The direction of skin folds hanging.

Maria

It is conceivable that Maria fell from a cliff and collided with the rocks, resulting in these injuries. In the sacroiliac joint on the right, two fragments of a foreign body are visible, presumably a stone (2150 HU on the Hounsfield scale), a bone defect and a lack of skin. The cavity above the foreign body is partially filled with mineral.

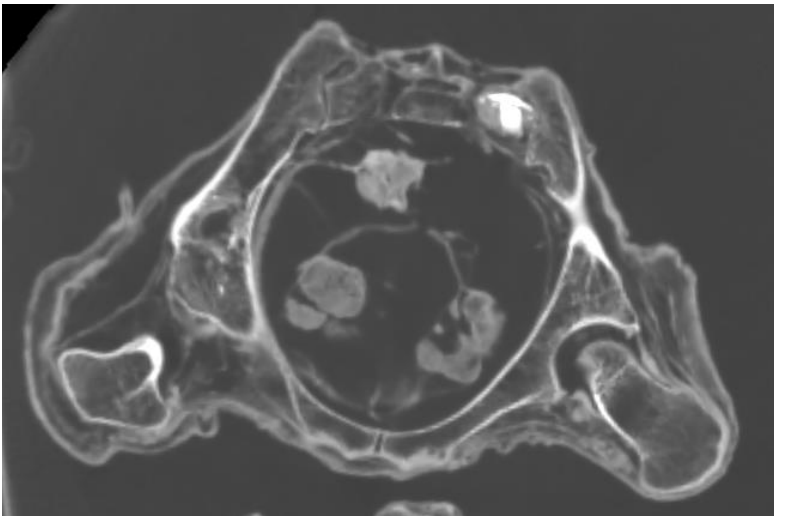

A foreign body was identified in the lumbosacral joint (horizontal plane).

It can be hypothesised that when the subject was in a lateral decubitus position, blood from the wound flowed down the buttock and accumulated in the area of the right hip joint and the wing of the ilium. It was in this area that a dense conglomerate of loose matter, measuring 96 by 68 mm in size and resembling a mineral in its dispersion and composition, formed.

Monserrat

When examining this area, a linear indentation on the skin is determined, similar to a mark left by a branch.

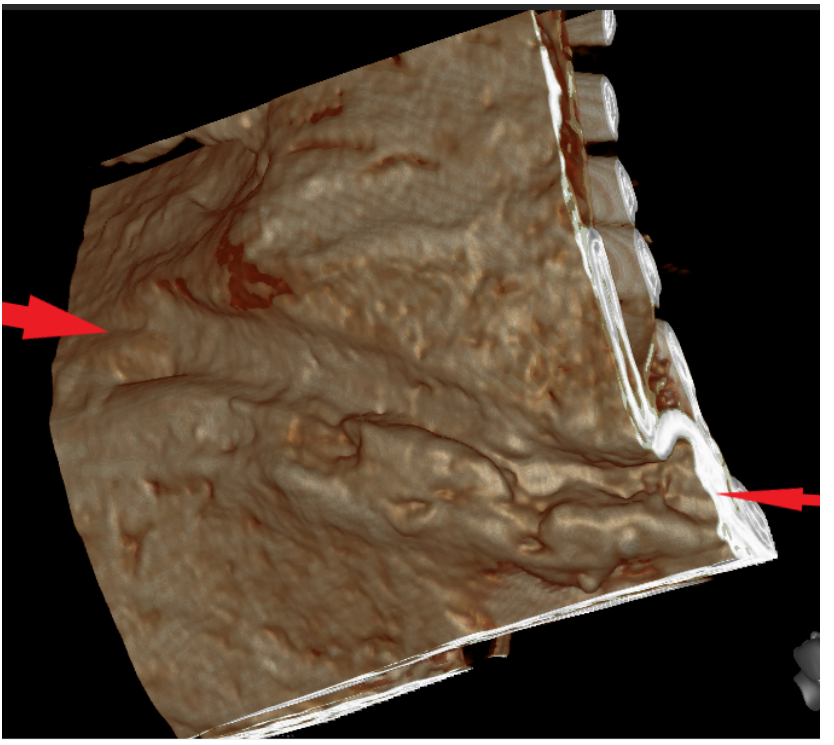

A mark left by a branch.

Post-processing of the radiographic images revealed the presence of several bone fractures, including those of the scapula and ribs. The wounds were most likely sustained shortly before or after death, since no callus formation is visible. The rotational movement of the upper fragment edge and the displacement of the scapular spine suggest that the cause of the trauma was from the interior.

Maria

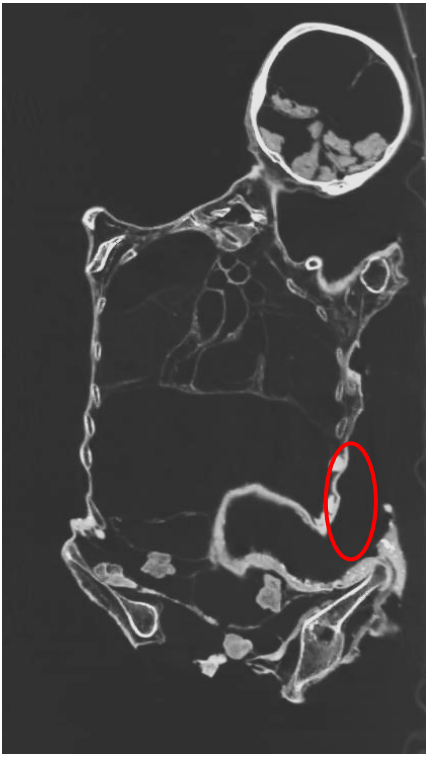

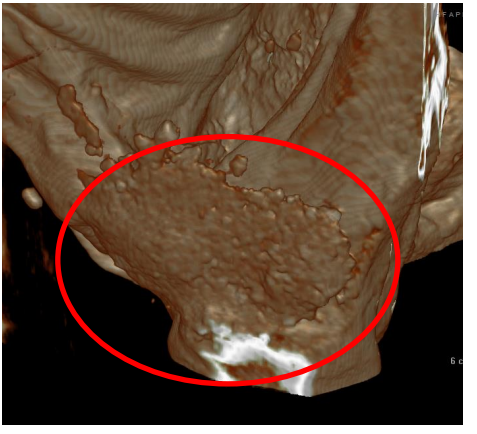

Dense conglomerate on the skin of the pelvis on the right.

Monserrat

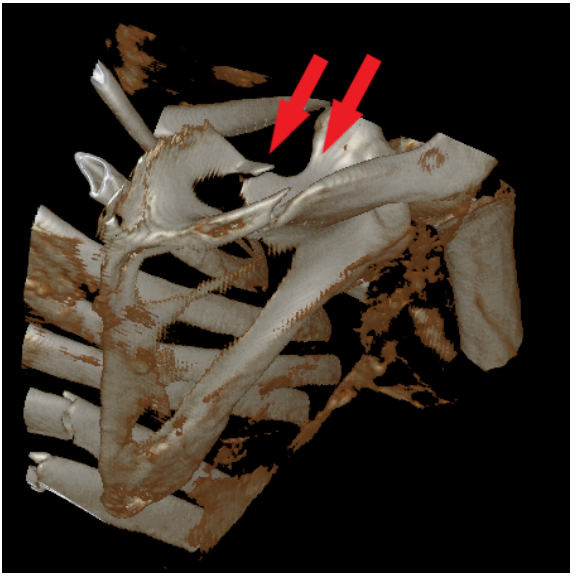

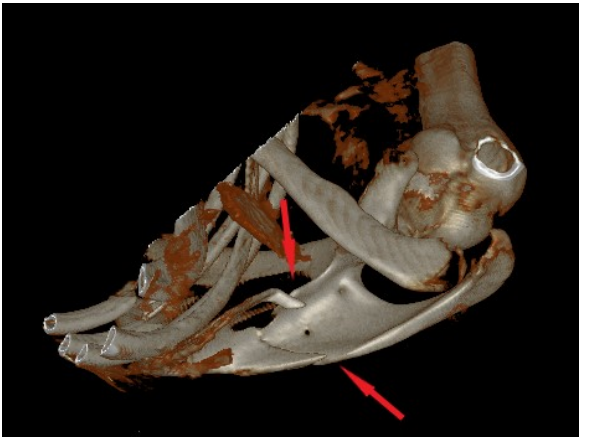

Fracture of the spine of the scapula and the upper edge in the projection of the notch of the scapula with displacement (indicated by the arrow).

Monserrat

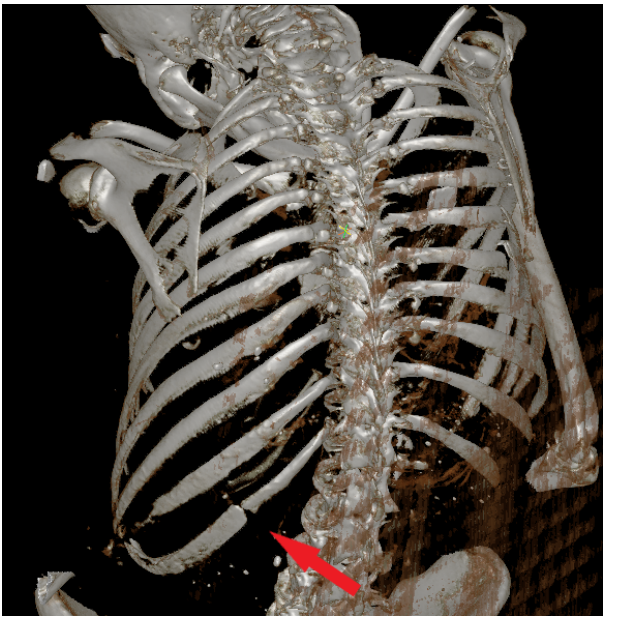

Fracture of the body of the 11th rib on the left.

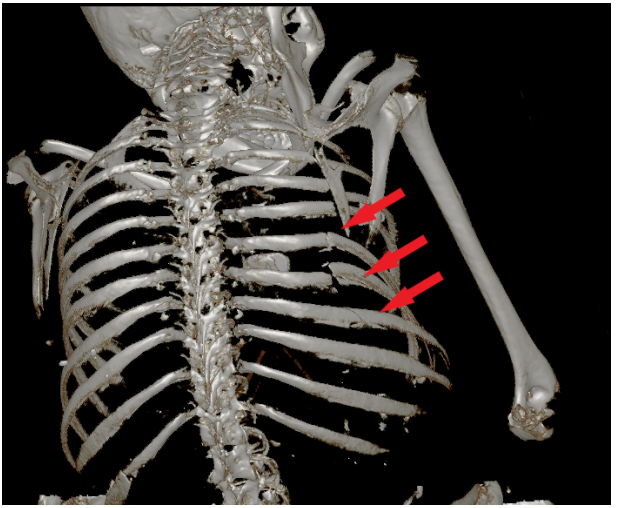

Fractures of the bodies of the 6th, 7th, 8th ribs on the right.

Monserrat

On the lateral surface of the chest on the left from the fourth to the ninth rib, significant oedema of the subcutaneous fat tissue is observed (which is presumed to be a haematoma). The same edemas – or hematomas, as they are also known – are found on the anterior surface of the abdomen.

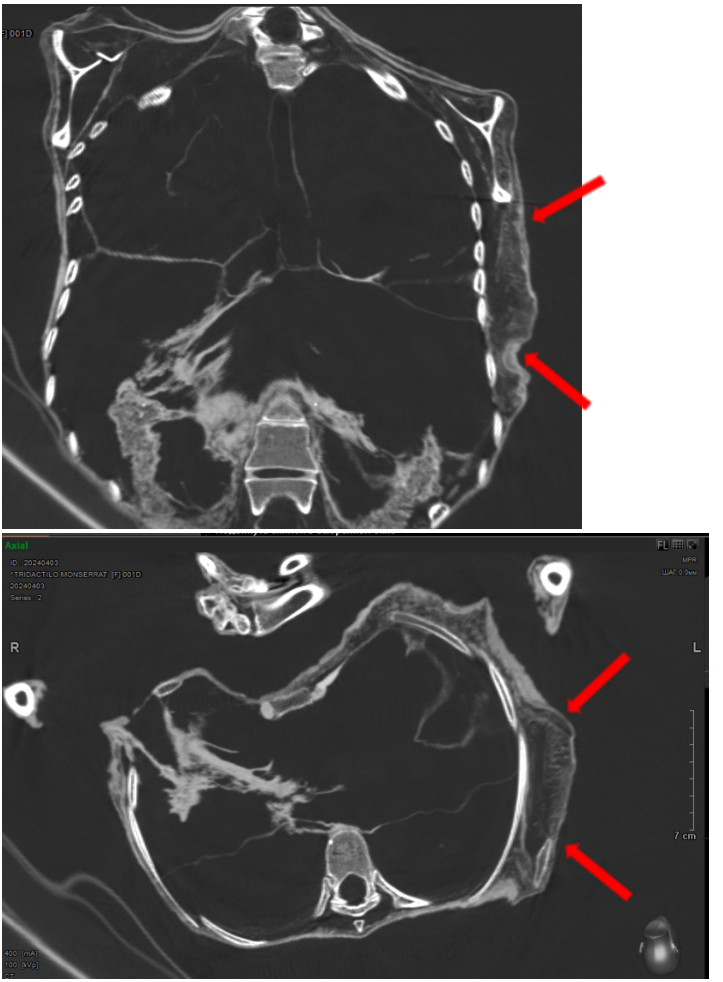

CT screens, frontal and horizontal reformat. Arrows indicate increased tissue volume on the lateral surface of the chest on the left.

Monserrat

In Montserrat's left hand, on the back of the right hand and on the chest, foreign bodies resembling metal in density are detected.

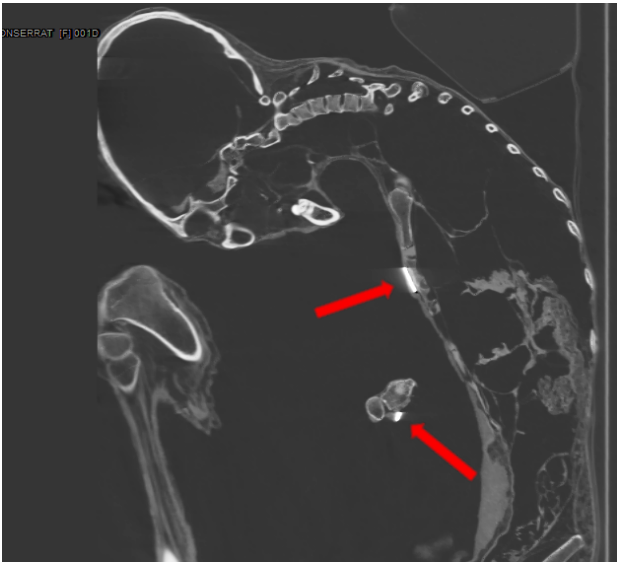

Foreign body in the left arm and chest.

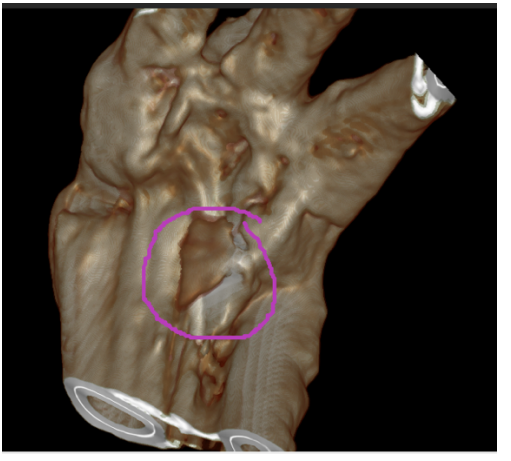

Foreign body in the left hand - reconstruction.

Monserrat

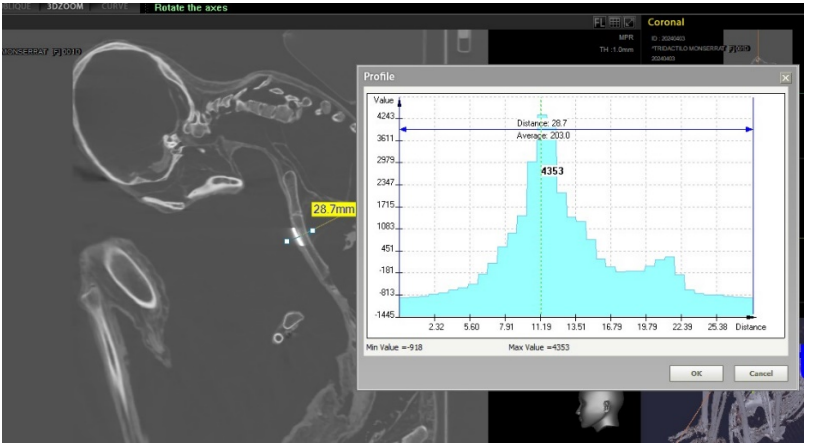

The evaluation of the density of an object on the chest was conducted using the Hounsfield scale (4353 HU. 4353 corresponds to the density of metal).

The presence of foreign bodies was detected on the head, in the frontal region, in the temporal regions, in the centre of the body of the sternum, and on the lateral surface of the chest on the right. The foreign bodies were observed to be round in shape, and square in shape, respectively. Finally, a foreign body was identified on the back of the right wrist.

Cranial construction

Maria

The cranium is of regular configuration, somewhat elongated in the anterior-posterior direction, the facial skull is flattened. The face is oval, the forehead is high, a pronounced frontal tubercle is defined.

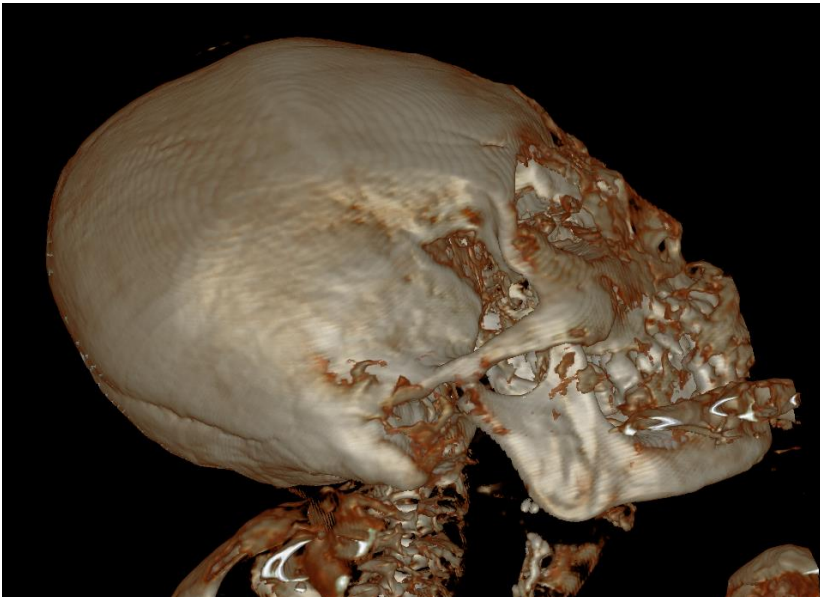

The lateral view of Maria's skull (reconstruction without soft tissues, post-processing) reveals that the eyes are closed and the structures of the orbit are distinguishable, including the eyeball, muscles and nerves. The eye slits are horizontal, and there is evidence of oedema in the area of the upper and lower eyelids of the left eye.

Monserrat

The cranium differs from that of individuals with normal anatomy - it is elongated in the anterior-posterior direction - signs of dolichocephaly.

Monserrat Skull Lateral View (Post Processing)

The skull bone structures are preserved. When examining the CT scans, a thinner bone is determined in the occipital region.

Maria

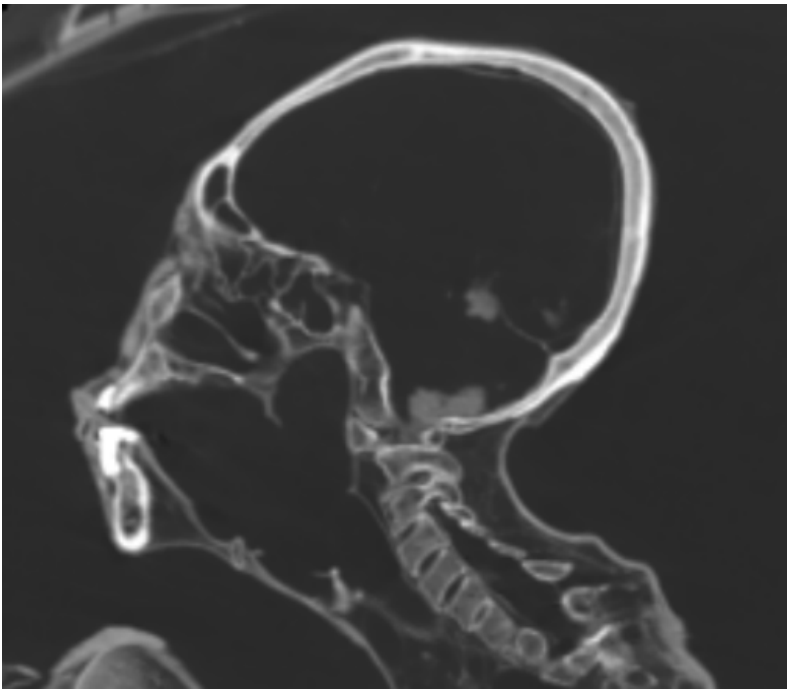

A CT scan in the sagittal plane reveals the presence of mineral fragments in the area between the eyeball and the eyelid. Maria's nose is of medium size. There is a swelling present in the nasal bridge region, accompanied by a rightward curvature of the nose. The mouth is closed, and of medium size. The lips are noted as thin. The presence of swelling in the upper left lip is also notable.

The paranasal sinuses are typically developed and air-filled. Radiopaque shadows are visible in the cranial cavity, indicating the presence of the remains of the brain.

Monserrat

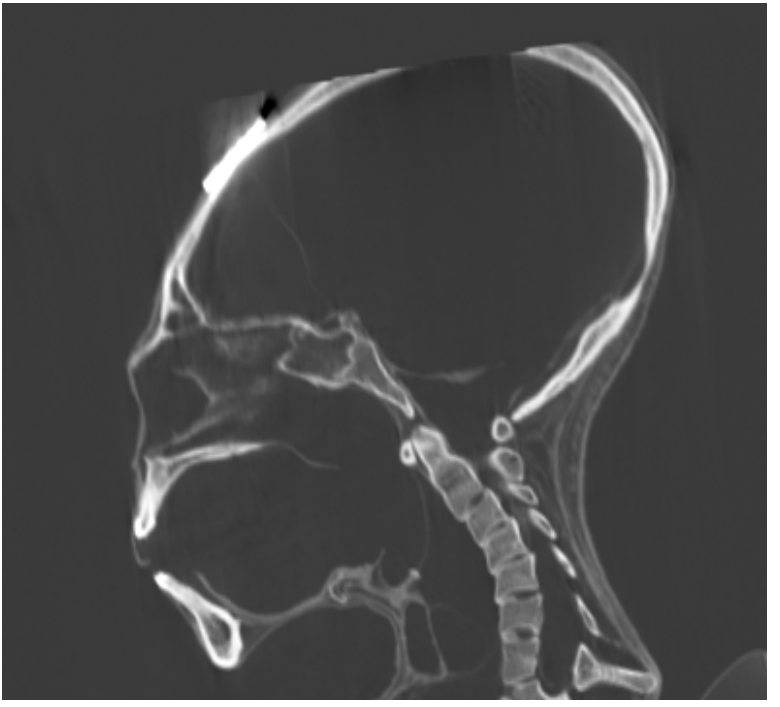

CT scan - sagittal plane.

The structure of the facial section of Montserrat differs from that of representatives with normal anatomy, as the facial section is flattened. The face is oval in shape, and the external nose is absent, as evidenced by the absence of nasal cartilages. The eye slits are located at an angle. A further observation, made during the examination of the tissues using CT, was that the nasal bones and cartilages were absent, and that the entrance to the nose was covered with skin from the nasal area. This is indicated by the transition with a step of tissues covering the entrance to the nasal passages. The mouth is observed to be in a slightly open position. The forehead is sloping. The sella turcica is positioned at a higher level.

Maria

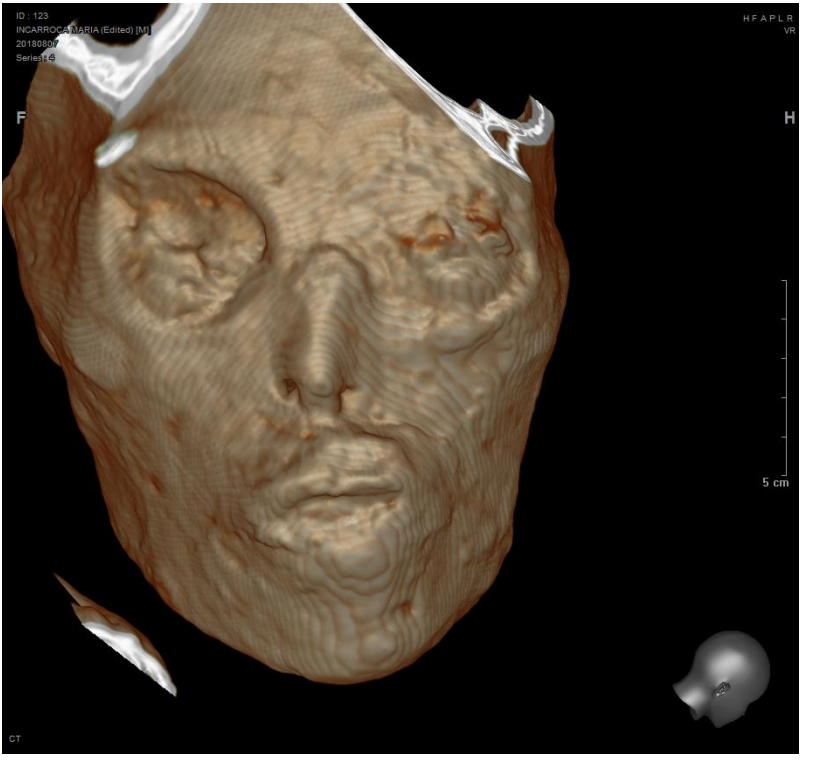

Face (reconstruction).

The following observations were made:
• swelling was visible in the area of the upper and lower eyelids of the left eye;
• displacement of the nose to the right;
• swelling of the lips; and
• swelling of the upper and lower eyelids of the left eye. It can be hypothesised that the injuries in these areas were sustained on the eve of death. Conversely, if the injuries had occurred after death, the swelling would have decreased within three days.

Furthermore, the presence of dehydration would have obscured these injuries, rendering them undetectable.

Monserrat

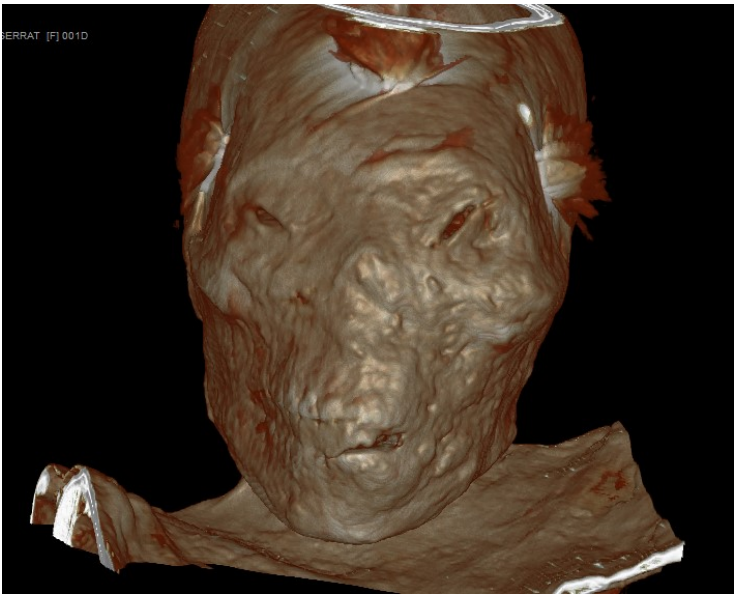

Face (reconstruction).

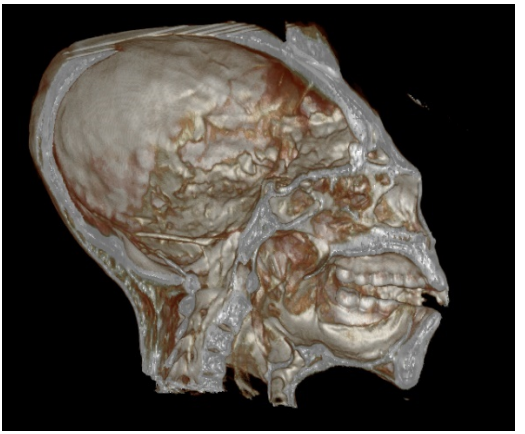

Scull reconstruction. Sagittal plane.

Maria

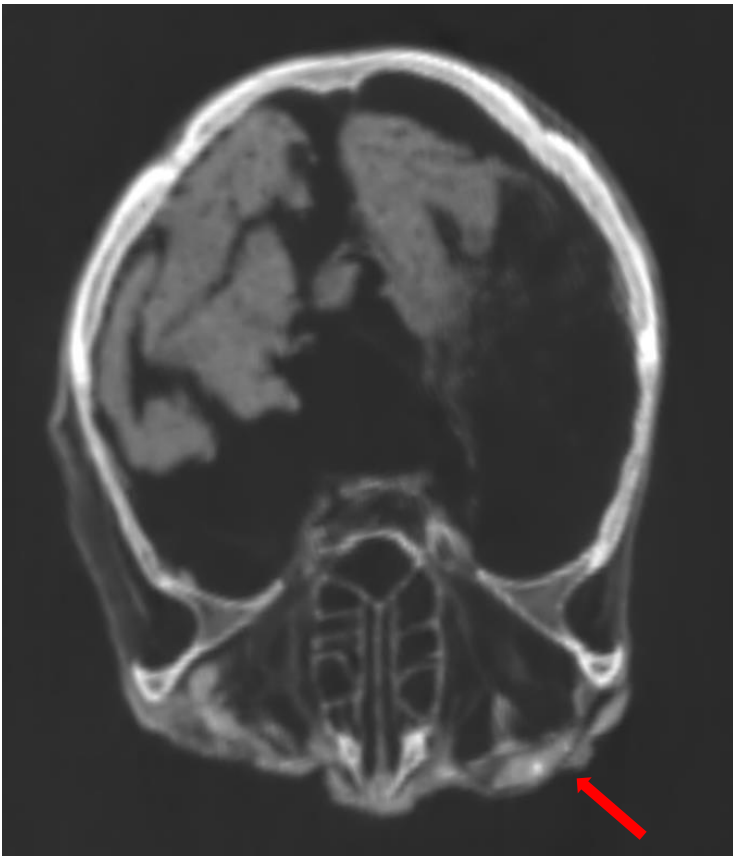

A mineral accumulation can be seen in the space between the eyeball and the eyelid. The auricles are missing, and there are no signs of forced removal. The external auditory canals are free.

Monserrat

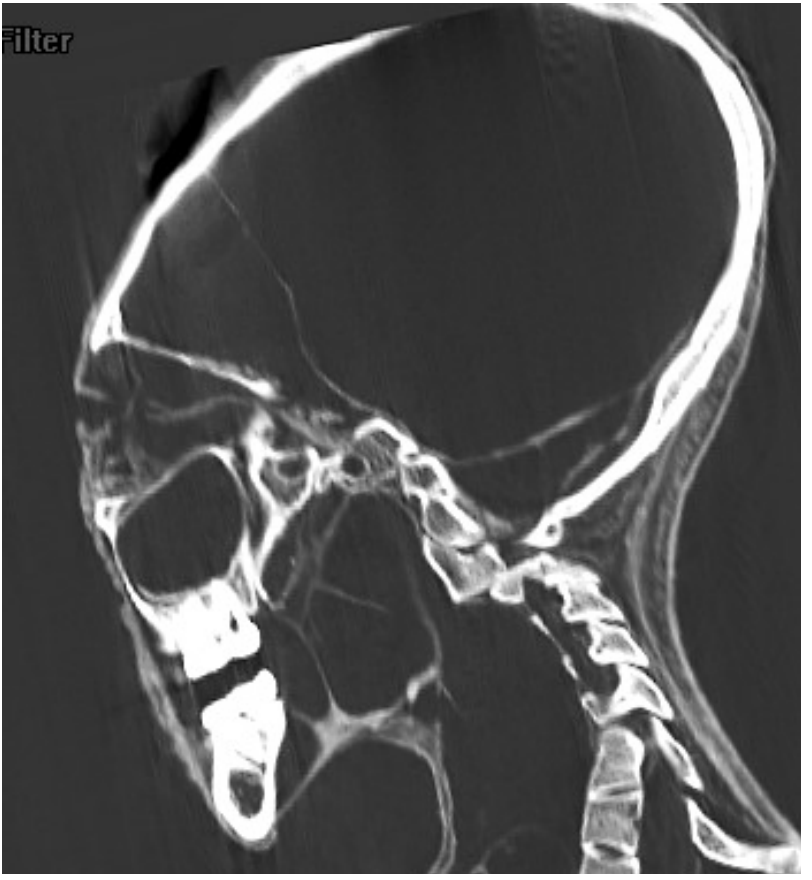

Orbital structures - CT screen oblique sagittal reformat, passing through the center of the right orbit. The structures of the orbit are visible - a dried eyeball, optic nerve.

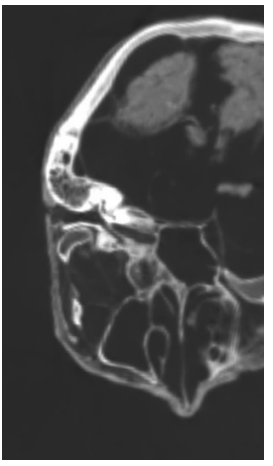

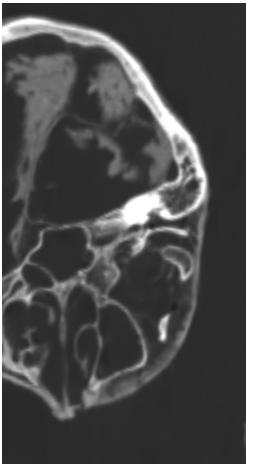

The external auditory canals are located in the region of the head and neck. Computer tomogram screens, horizontal plane. The paranasal sinuses are typically well-developed and air-filled. The nasal septum and nasal conchae are also within normal parameters. The temporomandibular joint shape is also within normal parameters.

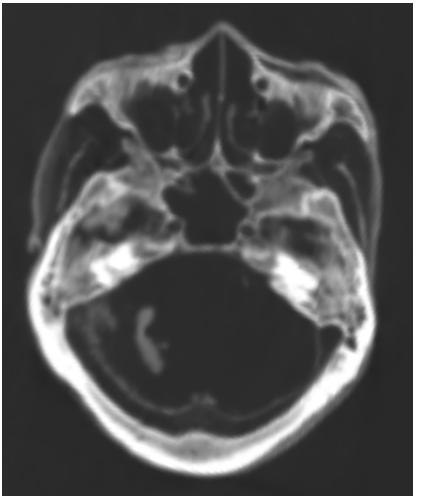

CT screen horizontal plane. Nasal-lacrimal canals are typical.

Monserrat

The paranasal sinuses are typically developed and airy.

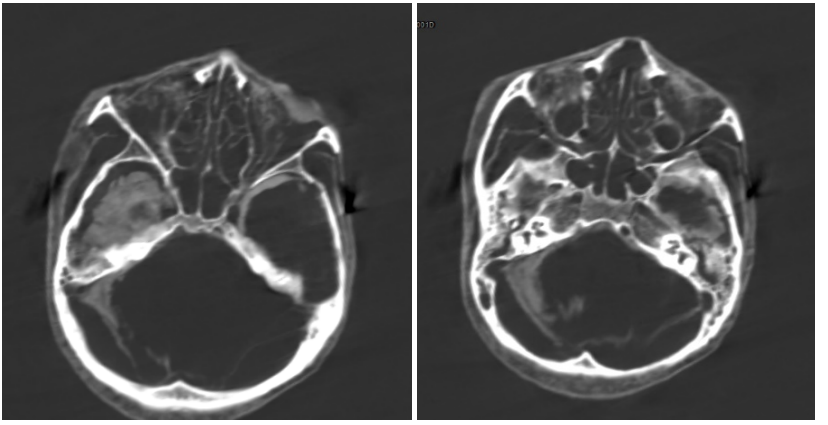

The following images depict a CT scan, viewed horizontally. The ethmoid and main sinuses are visible. Radiopaque shadows are visualised in the cranial cavity, indicating the presence of residual brain matter.

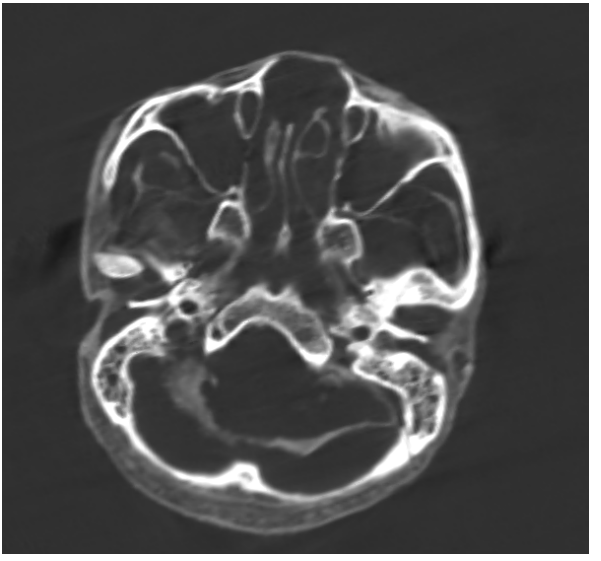

The external auditory canals are located in the following anatomical regions: The CT screen demonstrates a horizontal plane. Widened nasolacrimal canals are visible.

Maria

Radiopaque shadows are visible in the cranial cavity – the remains of the brain. The auricles are absent, and no indications of rough, violent removal are observed. The external auditory canals are unobstructed.

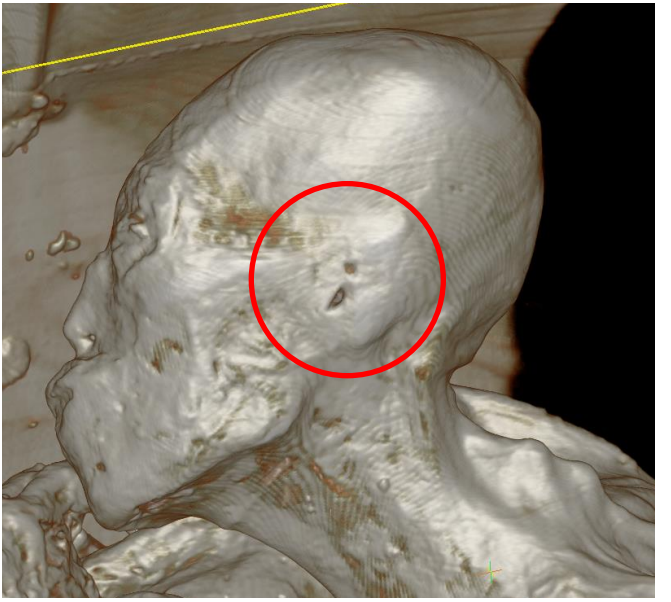

Monserrat

The auricles are absent, and no indications of rough, violent removal are observed. The external auditory canals are unobstructed.

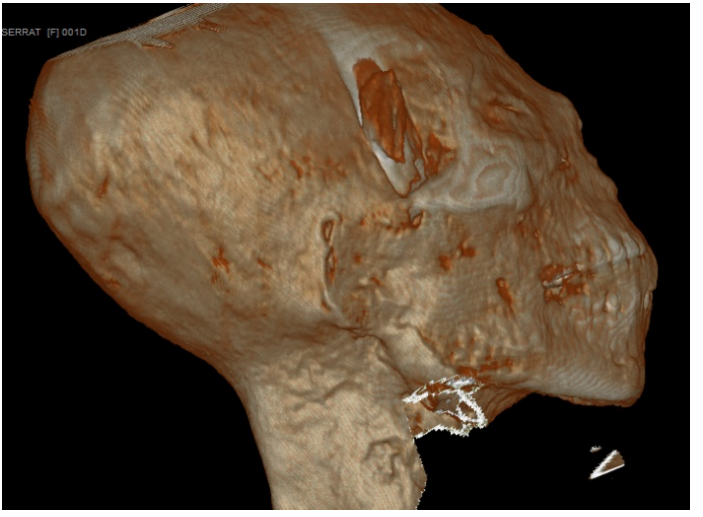

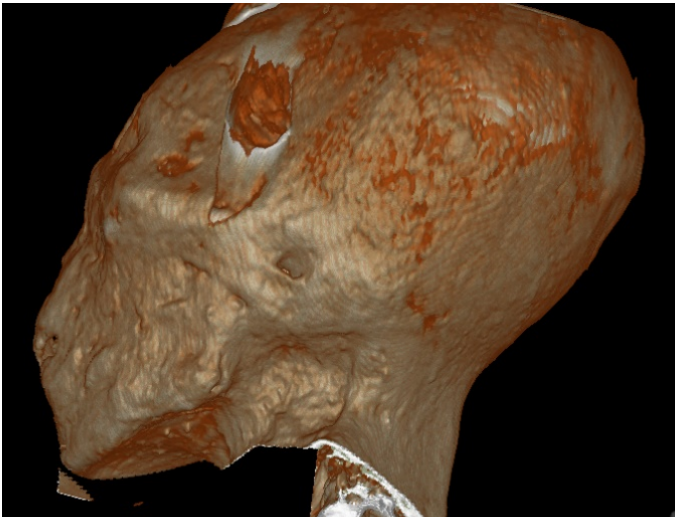

Monserrat

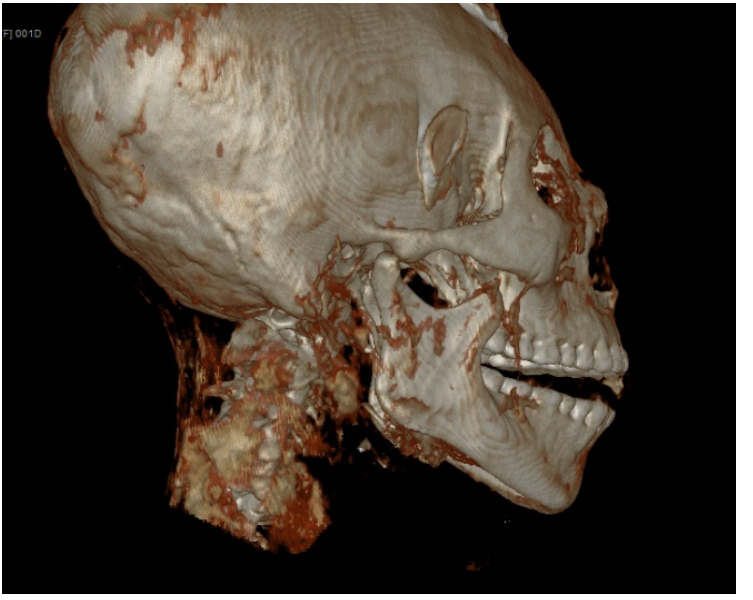

External auditory canal. Reconstruction without soft tissue.

Monserrat

Upon examination of the head, the atypical structure of the anastomoses of the maxillary sinus with the nasal passage is evident. Ordinarily, the maxillary sinus communicates with the middle nasal passage, a structure that is preserved in Montserrat, but is usually located at a higher level. Furthermore, additional anastomoses are observed along the upper margin of the inferior nasal conchae. The anastomoses themselves are located deeper in level.

In order to facilitate a more robust comparison, CT scans were obtained at the same level, allowing for direct anatomical comparison between Montserrat and a typical European subject.

Monserrat

Norm

Monserrat

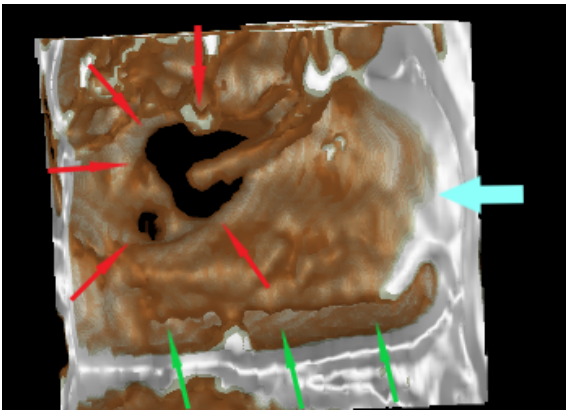

a

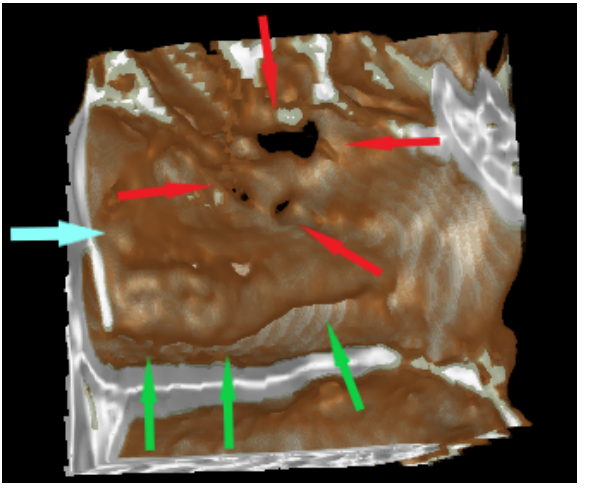

b

The following reconstruction of a fragment of the lateral wall of the nasal cavity with the nasal concha is presented: a – left nasal passage, b – right nasal passage. The communication with the maxillary sinus is indicated by red arrows. The inferior nasal concha's edge is indicated by green arrows. The direction of air inhalation is indicated in blue.

Monserrat

A thorough examination of the layered CT scans of the facial region reveals that the primary anatomical landmarks remain intact, though there is a notable widening of the nasal passages.

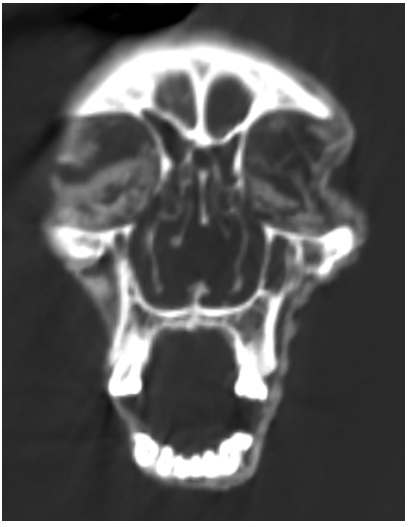

Monserrat

Norm

CT scans at the canine level.

Monserrat demonstrates widened nasal passages while maintaining the size of the bone structures of the septum and nasal conchae.

Maria

The following is a CT scan in the frontal plane. The image is taken at the level of the premolars. The CT screen displays the structures of the eye socket contents, including the eyeball.

The CT scan reveals that the bone structures of the subject's facial region are within normal parameters, as evidenced by the shape of the eye sockets, the structure of the maxillary and frontal sinuses, the location of the nerve exits (infraorbital and supraorbital), the structure of the nasal passages, and the structure of the alveolar process with teeth.

Monserrat

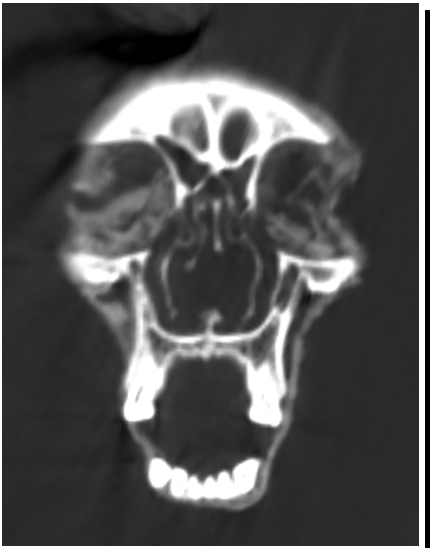

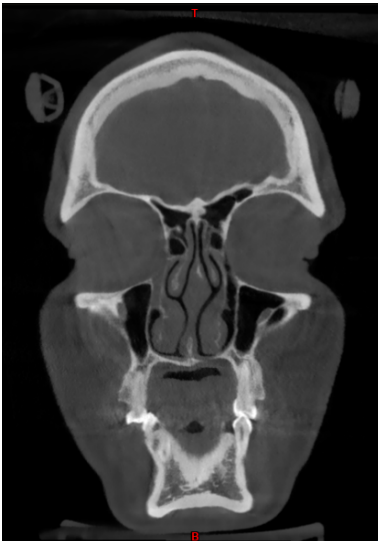

Monserrat Norm

CT scans at the premolar level.

Given the broad nasal passage observed, it can be hypothesised that Montserrat would have possessed a similarly broad nose. The absence of a nose can be hypothesised as either the result of an injury or damage due to an advanced disease, such as syphilis or lupus. However, no other traces of these diseases were detected.

Monserrat

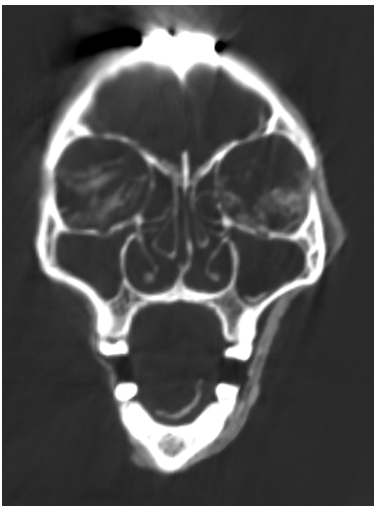

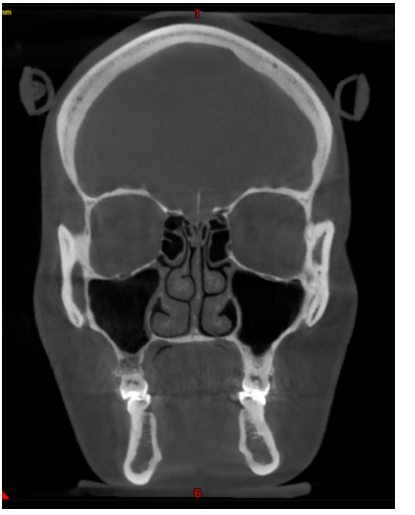

Monserrat Norm

CT scans, frontal plane. First molar level.

Monserrat Norm

CT scans, frontal plane. Third molar level.

Monserrat

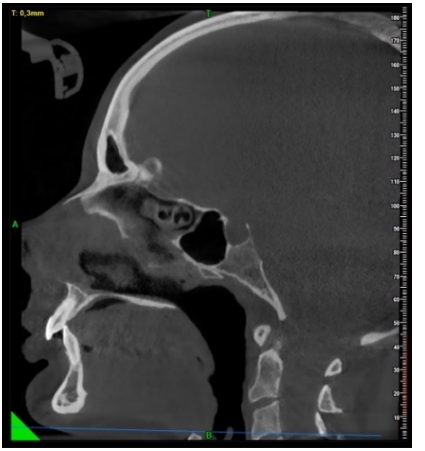

Monserrat Norm

CT screens sagittal plane. Vomer level.

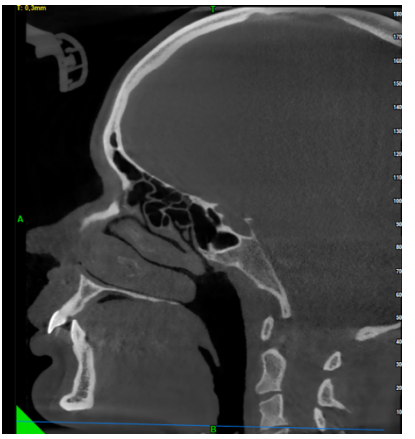

Monserrat Norm

Monserrat

The following investigation focuses on the level of the nasal conchae of the right nasal passage. In Montserrat, the presence of a bullous middle nasal concha (Concha bullosa) is observed. The naso-frontal articulation of the bones on the sagittal reformate is also characterised by the presence of unexpressed brow ridges and a sloping forehead. During the post-processing of the nasal area, a clear asymmetry of the nasal bones is visualised, creating the impression of destruction of these bones. The presence of an external nose is not evident.

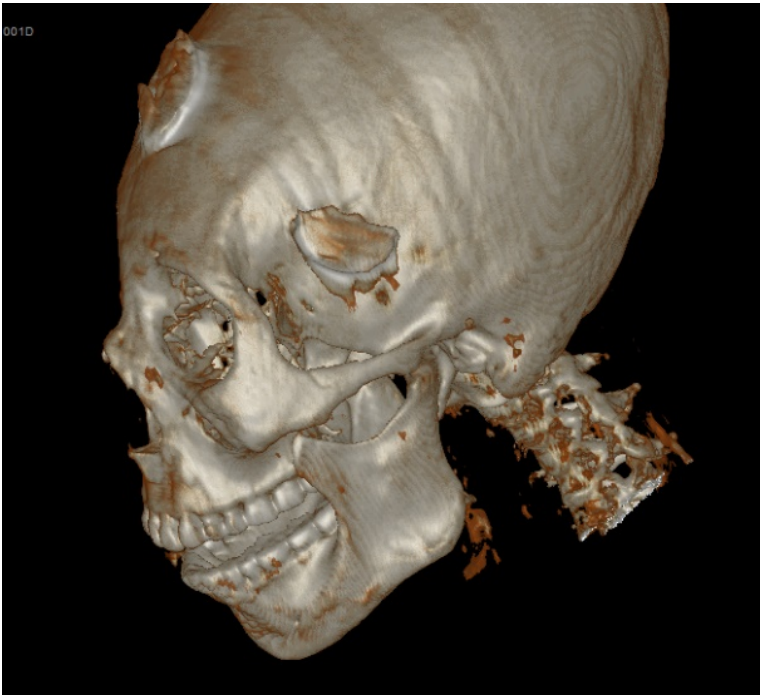

Monserrat

The nasolacrimal ducts exhibit marked dilatation, originating at the medial corner of the eye and opening into the lower nasal passage, as is customary.

Monserrat

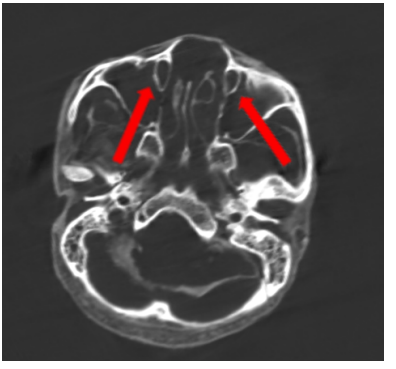

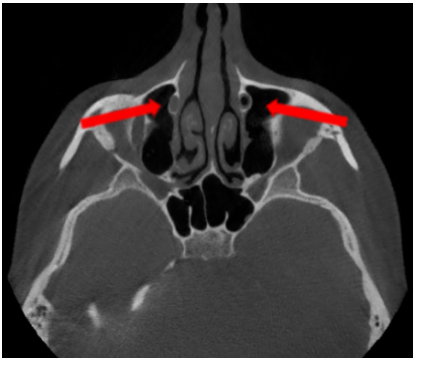

Монсерат Норма

CT scans. The duct is indicated by arrows.

Monserrat

The tongue is visualized in the oral cavity; the epiglottis and the entrance to the trachea are determined behind the root of the tongue.

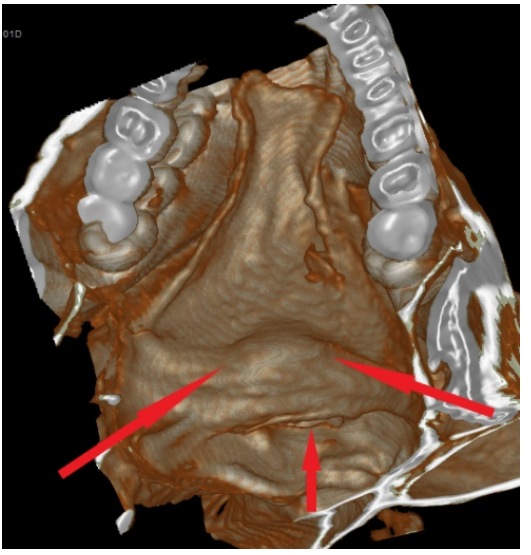

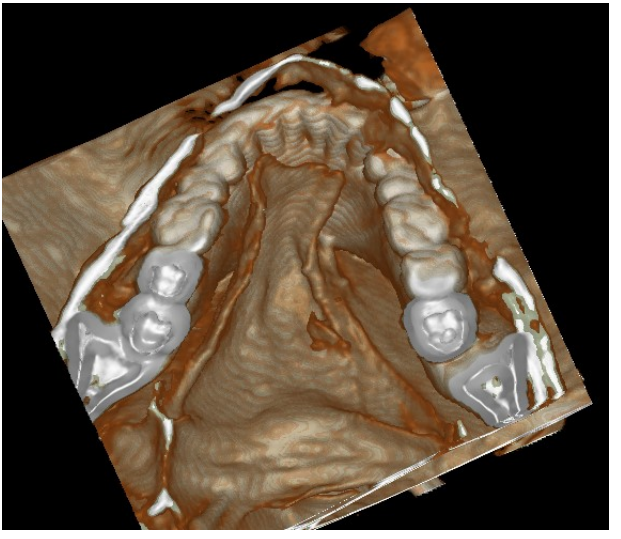

Reconstruction of a fragment of the lower jaw, the side arrows show the root of the tongue, the central arrow shows the entrance to the trachea.

Maria

The upper jaw exhibits the presence of three molars on the right side and two molars on the left. The remaining teeth are destroyed, exhibiting carious lesions and periodontitis at the apices of the root tips.

The lower jaw teeth are more thoroughly preserved, exhibiting three molars on the right and two molars on the left that are absent. The crowns of the remaining teeth exhibit wear to the extent of a quarter of their original size, and the presence of periodontitis is evident in the area of the root tips of teeth 31 and 32. A mineral accumulation is visible between the teeth and the mucous membrane of the cheek on the right.

Monserrat

The presence of a complete row of teeth, exhibiting minimal wear and no signs of caries, suggests that the subject is a young adult female. The jaws exhibit a typical structure, with a compaction observed in the body of the lower jaw on the right, between the roots of teeth 42 and 43. This compaction is presumed to be cement.

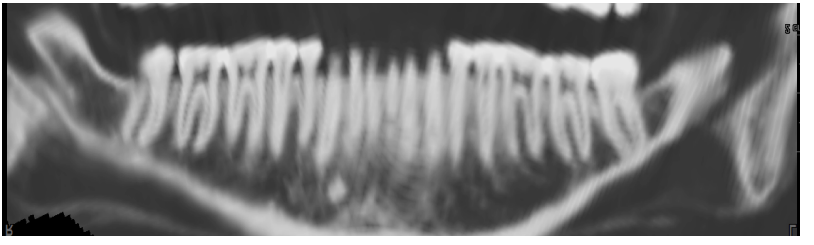

The roots of the teeth are longer than those of the average person.

Maria

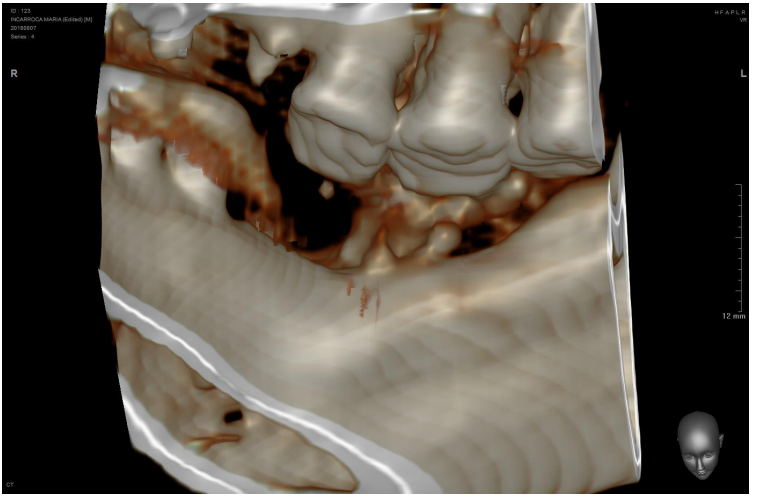

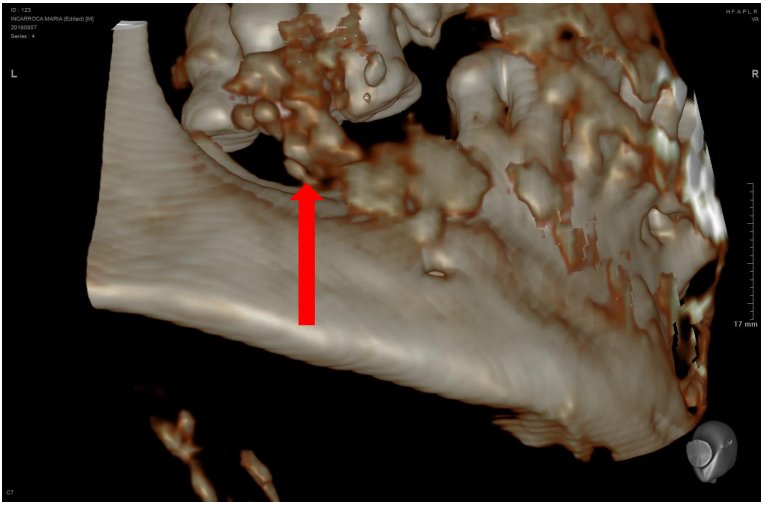

Mineral accumulation between the teeth and the mucous membrane of the cheek on the right.

Body construction

Maria

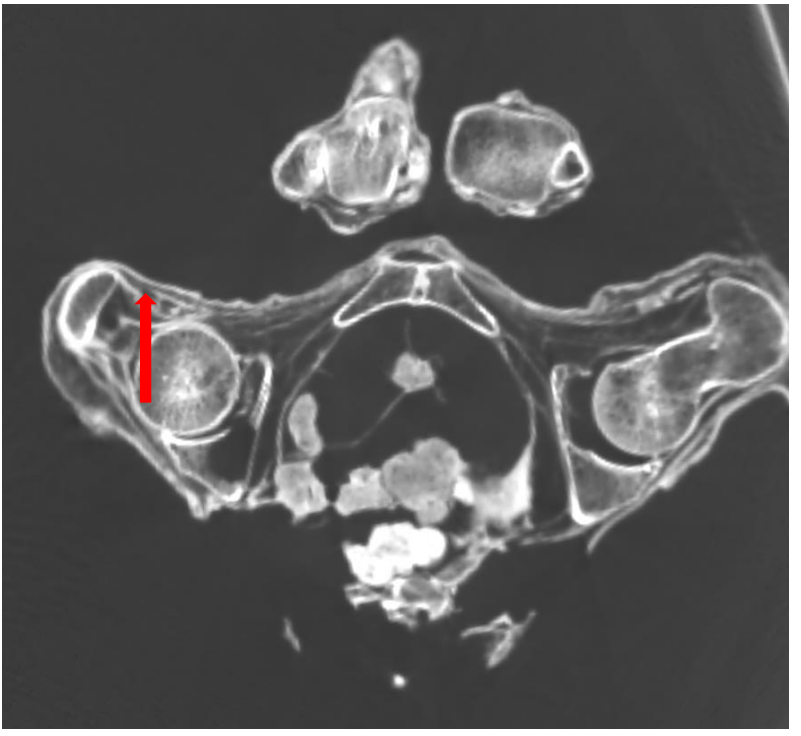

Destruction of bone tissue (horizontal plane))

Maria

All bone structures and their articulations that are characteristic of the human skeleton are present and typically developed. The vertebrae and spinal canal exhibit a classic configuration, and the number of vertebrae in the spinal column corresponds to the human skeleton (7 cervical, 11 thoracic and 5 lumbar, 5 sacral).

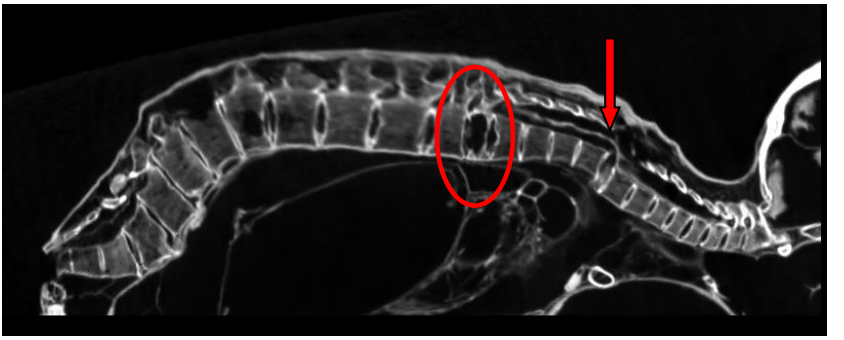

Displacement of the bodies of the second and third thoracic vertebrae is evident, as is oedema of the interarticular disc (indicated by the arrow). A cavity is also present in the area of the body of the seventh thoracic vertebra (circled) (sagittal plane). The displacement of the bodies of the II and III thoracic vertebrae is evident, accompanied by edema of the interarticular disc. A cavity corresponding to a hemangioma is also visible in the area of the body of the VII thoracic vertebra.

The cavity in the region of the body of the 7th thoracic vertebra (horizontal plane).

Panoramic reconstruction of the spinal column and CT scan of the 7th thoracic vertebra, horizontal plane.

Monserrat

The neck is of medium length, thin, and unmarred. The chest is flat-cylindrical in shape and exhibits a symmetrical configuration. Consistent with the typical configuration observed in the general population, the sternum, cartilages and ribs are present, exhibiting the appropriate number and shape within the anatomical norm.

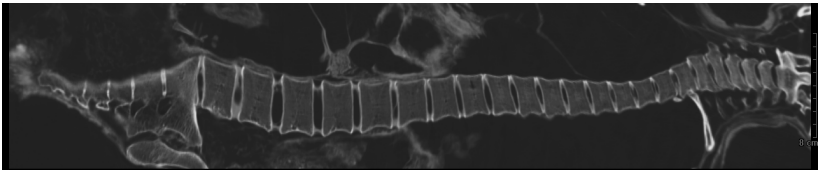

The absence of beak-shaped growths on the vertebral bodies serves to corroborate the supposition that the woman is of a juvenile age. All bone structures and their joints that are characteristic of the human skeleton are present and developed typically. The vertebrae and spinal canal exhibit a conventional configuration, with the number of vertebrae in the spinal column corresponding to the human skeleton (seven cervical, 11 thoracic, and five lumbar vertebrae, along with five sacral vertebrae, of which the fifth is composed of three fused vertebrae).

Panoramic reconstruction of the spinal column and sacral region

Maria

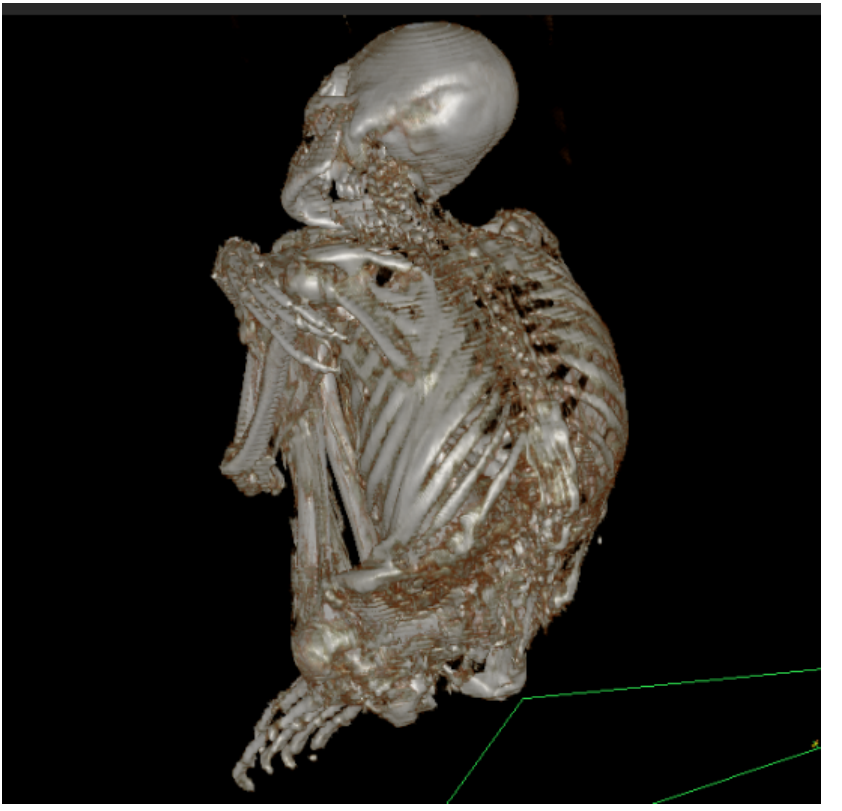

Maria's rib cage is characterised by its flat, cylindrical and symmetrical configuration. It consists of all the principal elements – the sternum, cartilages and ribs – the number and shape of which correspond to the established anatomical norms.

The image depicts the reconstruction of Maria's thoracic and lumbar spine.

Monserrat

Reconstruction of the thoracic and lumbar spine.

The rib cage is flat-cylindrical in shape and exhibits bilateral symmetry. Consistent with the configuration observed in typical individuals, the rib cage comprises the sternum, cartilages, and ribs, the numerical quantity and configuration of which align with anatomical norms.

Maria

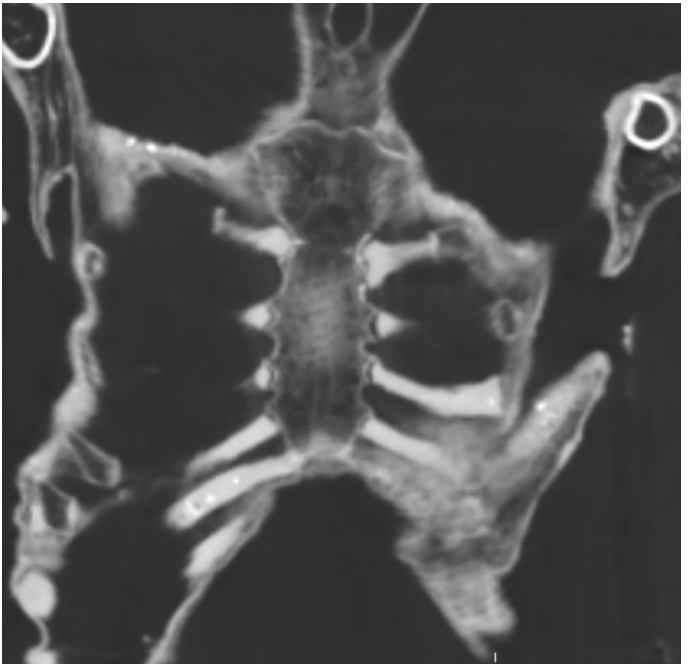

The structures of the sternum are preserved and have a classic shape.
CT scan of the body and manubrium of the sternum.

Monserrat

Inside the body of the sternum there is a cavity with partitions.

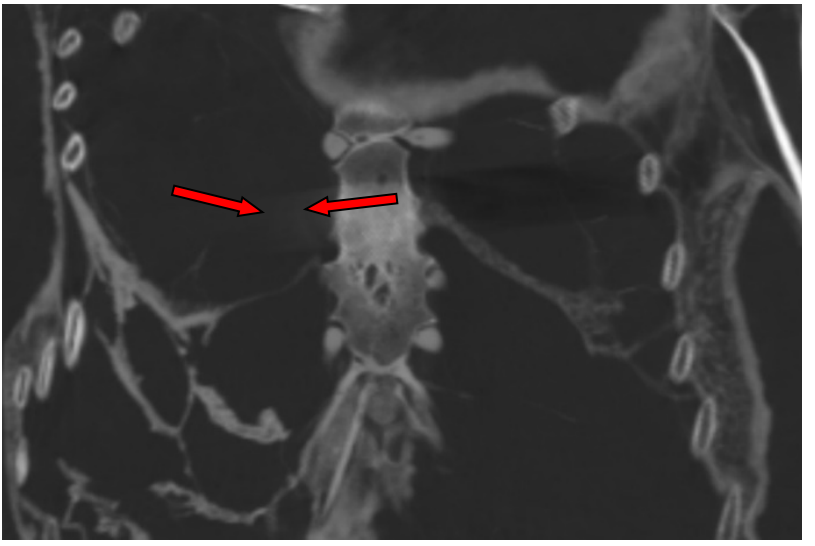

CT scan, showing the body of the sternum with cavities.

All structures of the sternum are preserved and have a classic shape.

Maria

On the right side, at the level of the 4th intercostal space, a fold of skin is visible, corresponding in appearance and location to the mammary gland. The nipple is not clearly delineated. On the left side, the mammary gland is not visualised.

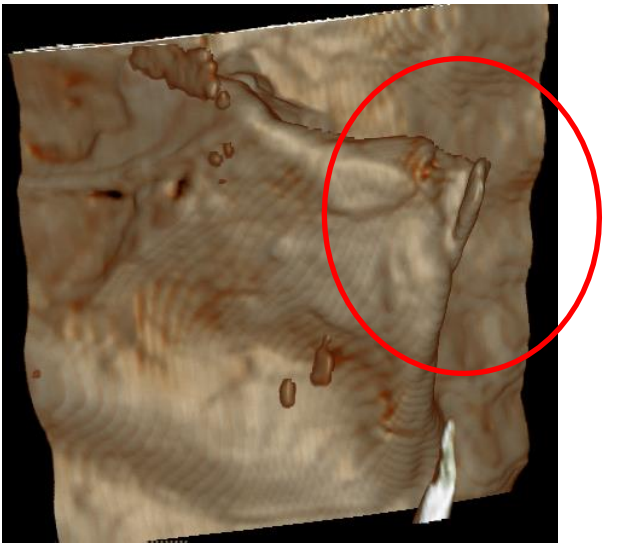

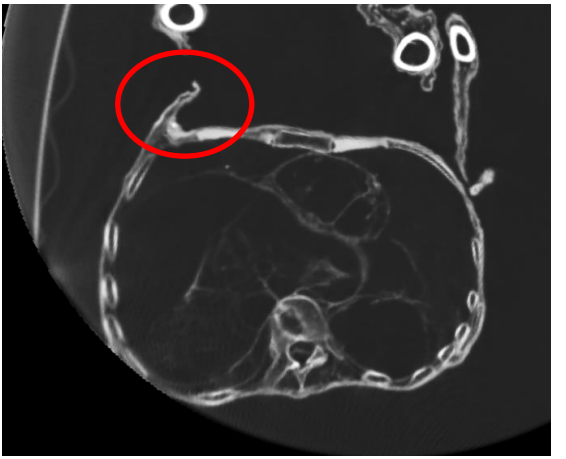

Reconstruction and CT scan of the mammary gland, horizontal plane on the right.

Monserrat

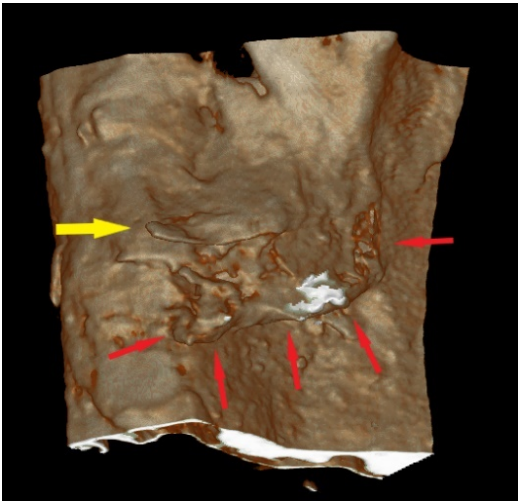

As illustrated in the sixth and seventh rib projections on the right, there is a conspicuous protrusion of the skin corresponding to the mammary gland – the nipple (yellow arrow). Beneath this, there is an exophytic formation with multiple violations of the skin's integrity, which may be indicative of a tumour in the mammary gland with decay. The delineation of these boundaries is indicated by the red arrows. It is evident that there is growth into the pleural cavity, as evidenced by the presence of HER2-positive tumours. It is important to note that pregnancy, Montserrat, and significant hormonal changes in this context can not only result in accelerated tumour growth and its subsequent spread into the chest cavity, but also lead to the emergence of metastases in the colon, potentially resulting in obstruction (as indicated by the filled colon).

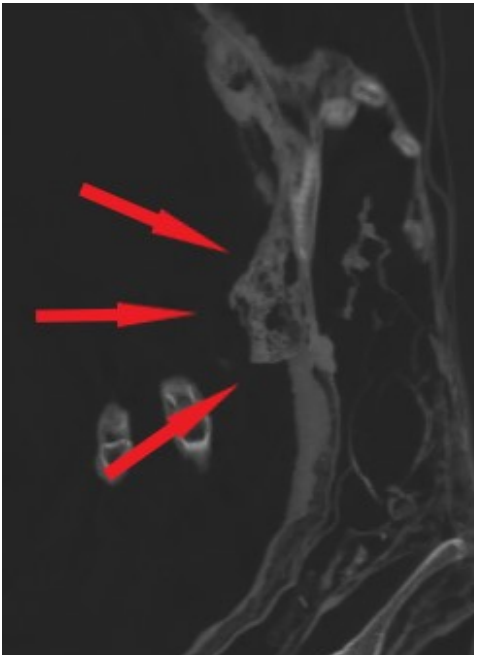

Reconstruction and CT screen of the sagittal plane of the mammary gland and tumor on the right.

Maria

When examining the neck, the tissues of the trachea, esophagus, and epiglottis are clearly visible.

CT screen sagittal reformat. The laryngopharynx, trachea and upper esophagus are united by an oval.

Monserrat

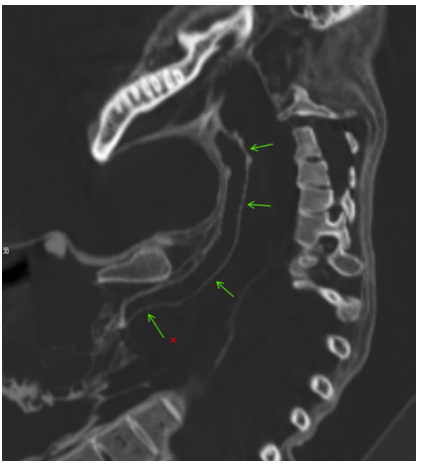

Upon examination of the neck region, the presence of cartilaginous rings becomes evident in the tracheal tissues, thereby facilitating their distinction.

CT scan, oblique sagittal plane. The posterior wall of the trachea is indicated by the arrows. The lumen of the esophagus is delineated posterior to the trachea. It has been observed that, during the process of mummification, there is a flattening of the paravertebral and parapharyngeal tissues. This is believed to result in the stretching of the oesophageal tissues, which are significantly expanded on CT scans.

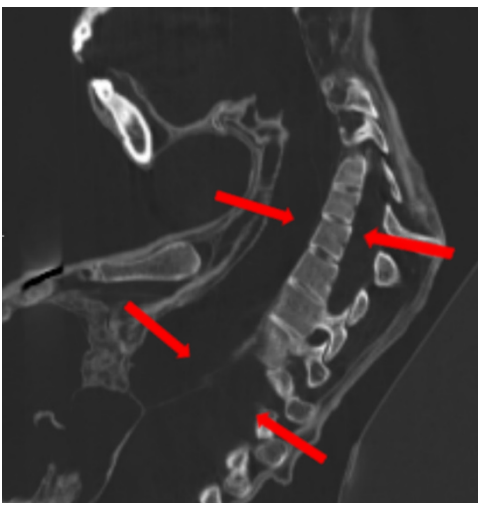

CT screen sagittal plane. The walls of the trachea are indicated by arrows.

Maria

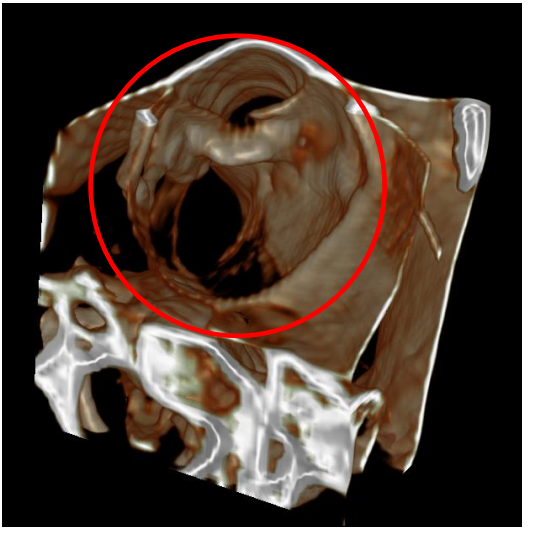

Post-processing - reconstruction of the epiglottis, entrance to the trachea and esophagus.

Monserrat

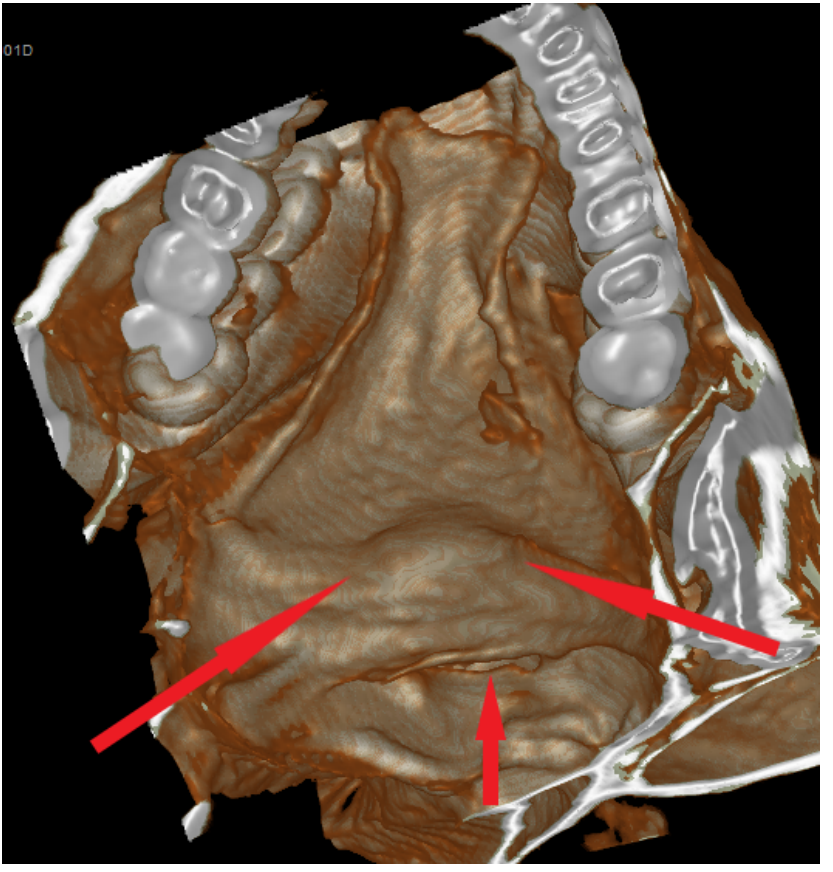

Post-processing allows the epiglottis and the entrance to the trachea and esophagus to be distinguished.

Maria

The heart is delineated within the chest cavity, with clearly defined contours of the heart chambers, indicative of their correct configuration (illustrated by the arrow). All the heart chambers are clearly visible, and it appears that following death, they were filled with blood. Such a postmortem change may be indicative of slowly developing chronic heart failure. The bronchial tree (large bronchi) has been delineated. Lung tissue is visible.

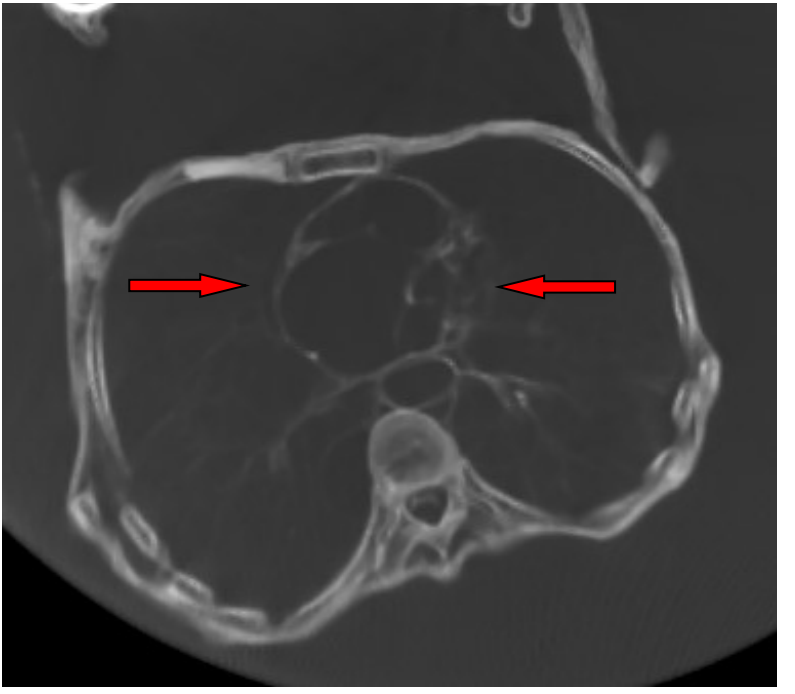

CT scan of the patient's abdomen was performed in a horizontal plane. The chest and the heart.

In the region beneath the diaphragm, the presence of liver tissue, mesentery, and dense radiopaque contents within the intestinal loops becomes discernible. However, it should be noted that the kidneys, ureters, bladder, and gynaecological organs are not visualised.

Monserrat

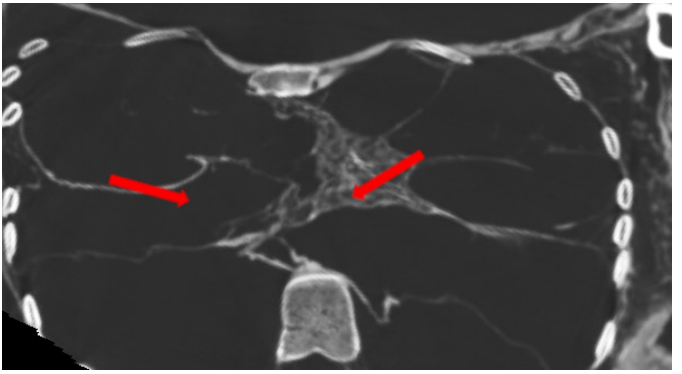

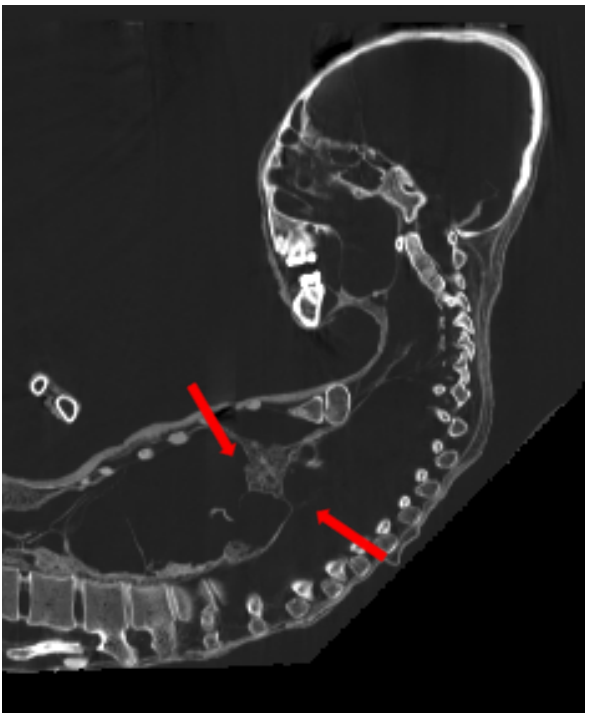

CT scans, horizontal plane and sagittal plane – the heart is indicated by the arrows. The cardiac silhouette is discernible in the chest region; however, the cardiac chambers remain indistinct due to the collapse of the heart, which appears to be a conglomerate of tissues. This phenomenon, known as the heart's last breath, has been observed in cases of sudden cardiac death, typically characterised by a cardiac arrest.

Maria

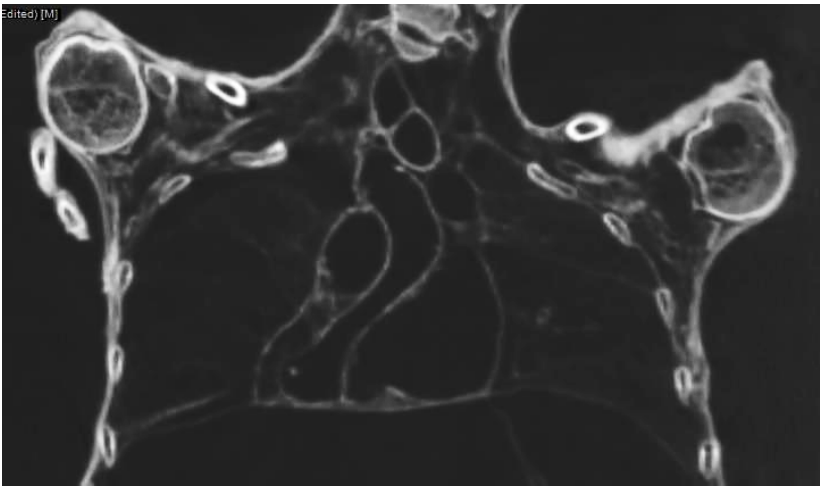

CT scan screens frontal plane. Chest, heart.

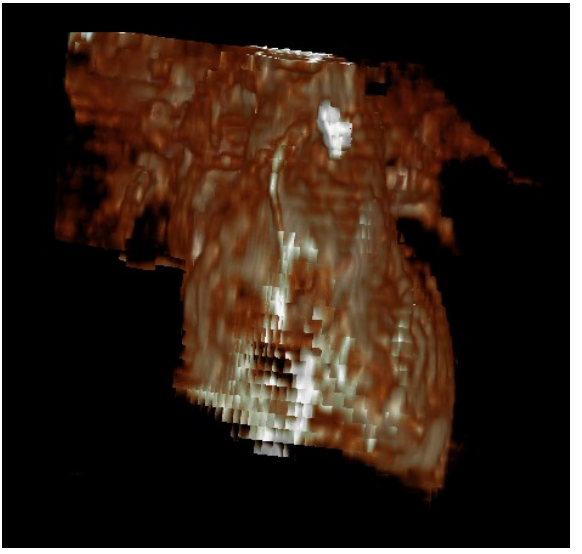

Heart reconstruction.

Monserrat

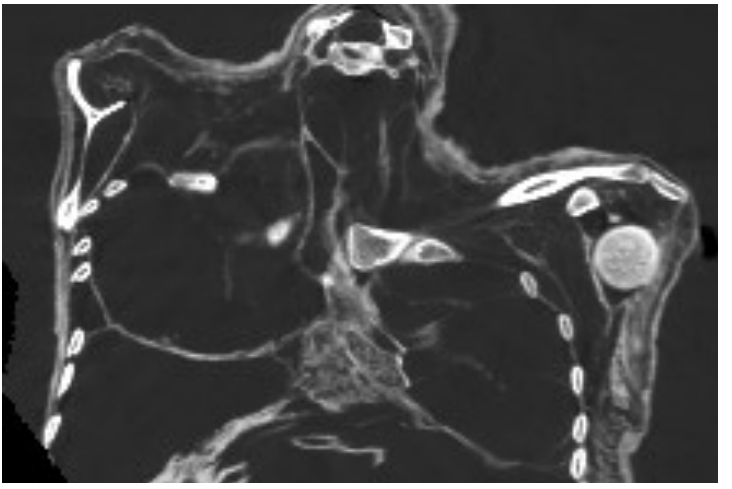

CT scan screens frontal plane. Chest, heart.

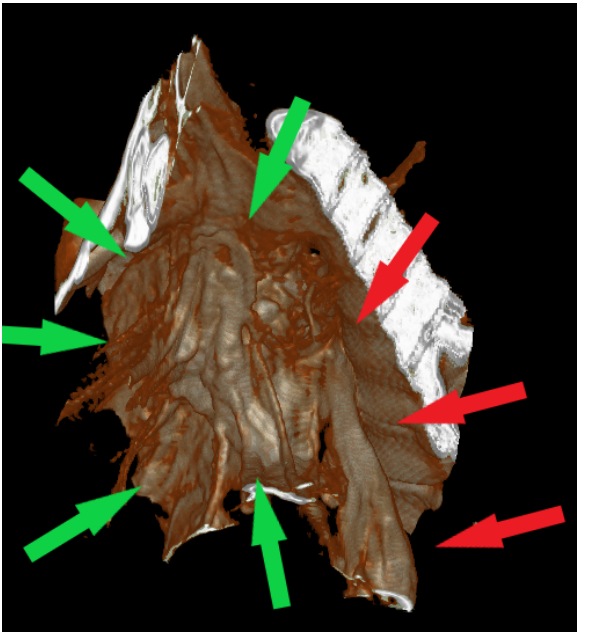

Heart reconstruction, green arrows indicate the contour of the heart, red arrows indicate the descending aorta.

Maria

A thorough examination of the abdominal cavity is the only way to ascertain the presence of the liver (see circled area). During the process of dehydration, the substance undergoes a change in its shape and its structure is altered, yet its position remains unaltered.

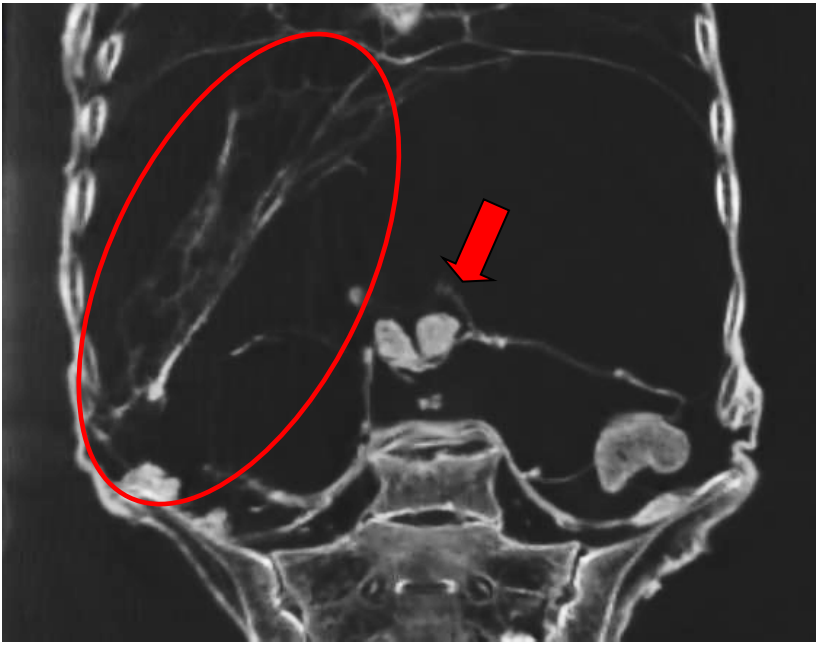

CT scan of the abdominal cavity - frontal plane.

Further examination allows us to see the mesentery and intestines with dense inclusions of fecal matter (indicated by the arrow). The search for kidneys did not yield any results, and we assume that this is a consequence of both their small size and compression due to dehydration. And their location outside the abdominal cavity - in the retroperitoneal tissue complicates their differentiation after dehydration.

Monserrat

In the area beneath the diaphragm, the liver tissue and mesentery are clearly discernible. In the intestinal loops, there are inclusions of dense radiopaque contents. The kidneys, ureters and urinary bladder are not visualised.

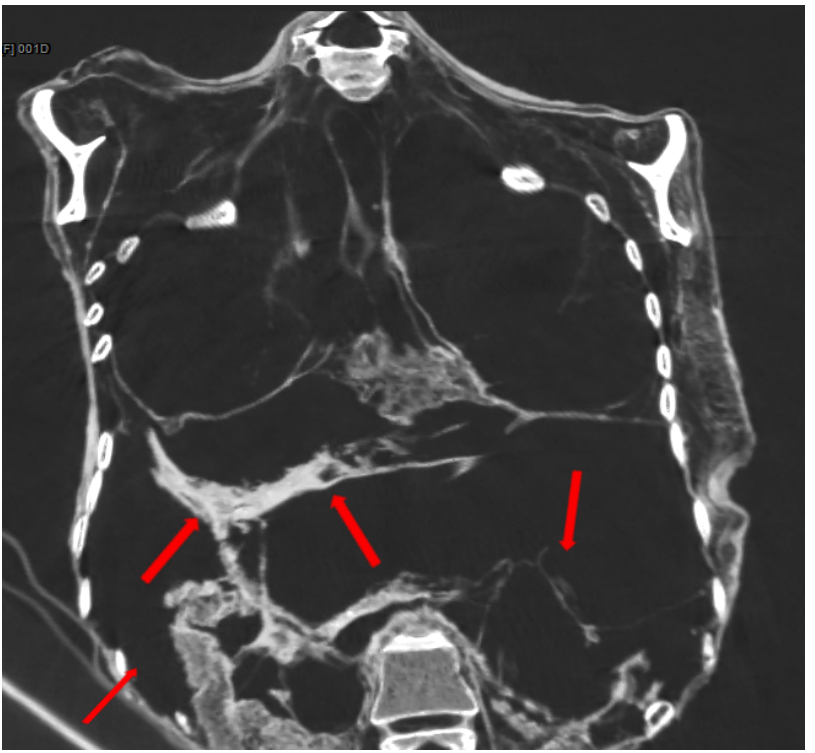

The CT scan image in the frontal plane demonstrates the presence of liver tissue, the ascending colon, and mesenteric tissue, as indicated by the arrows.

As previously mentioned, upon examination of the liver, a rupture of its tissues was determined at the level of the 5-6 rib (presumably a stab wound). In cases of dehydration, the visualisation of the lesion is enhanced due to the divergence of the edges.

Monserrat

In the projection of the large intestine with a significant amount of fecal matter, a dense object is visualised; with post-processing, it can be determined that this is a seed of the plant that Montserrat consumed prior to her demise.

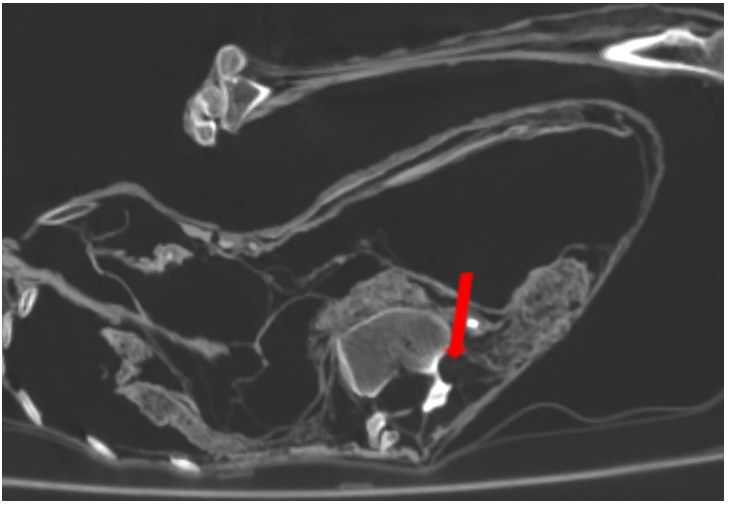

CT scans of the abdominal cavity - frontal and horizontal plane. The seed is indicated by the arrow.

Monserrat

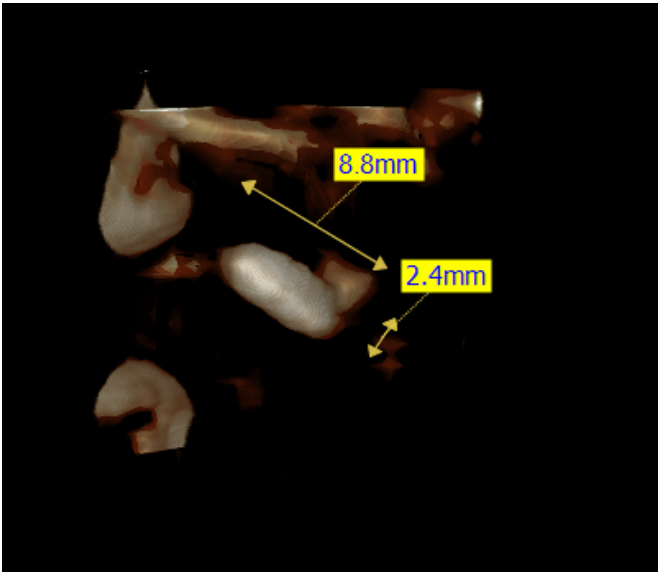

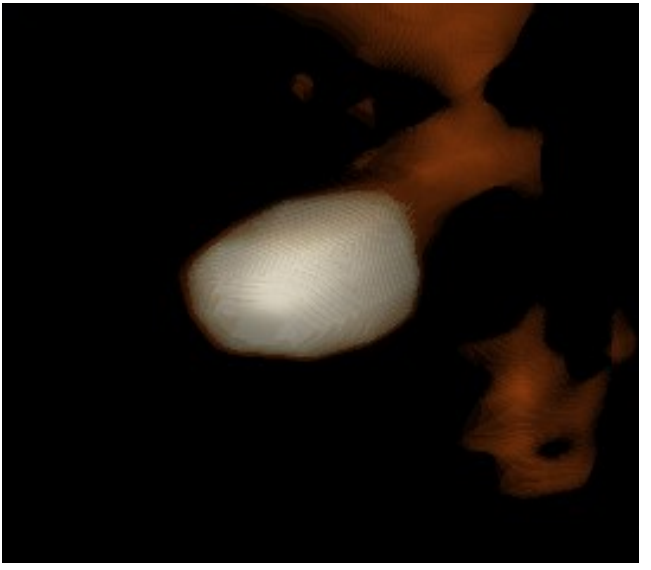

Reconstruction of an object in the intestine during post-processing.

Skeletal system

Maria

The bones of the clavicle, scapula, shoulder, forearm, and their joints have a classic configuration.

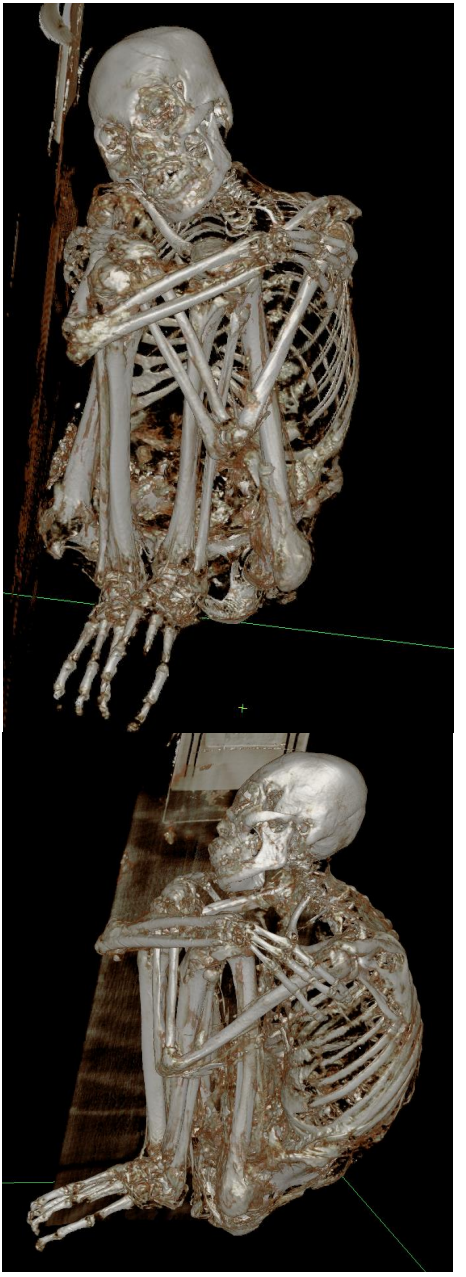

Post-processed reconstruction of Maria's skeleton.

Monserrat

The bones of the clavicle, scapula, shoulder, forearm, and their joints have a classic configuration.

Post-processed reconstruction of Monserrat's skeleton.

Maria

The bones of the pelvis and hip, along with their respective joints, exhibit a conventional arrangement. The structure of the bones is standard, with the cortical layer expressed in the tubular bones. As a consequence of the injury sustained, there is a clear infringement of the structural integrity of the bones and soft tissues of the small pelvis.

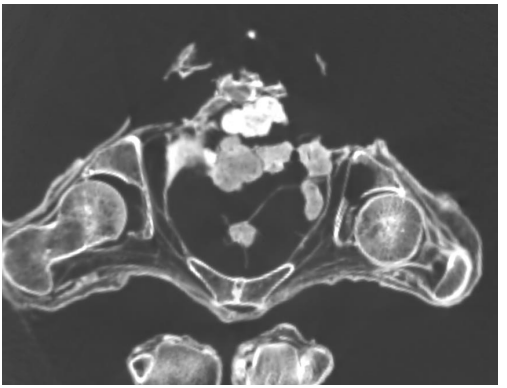

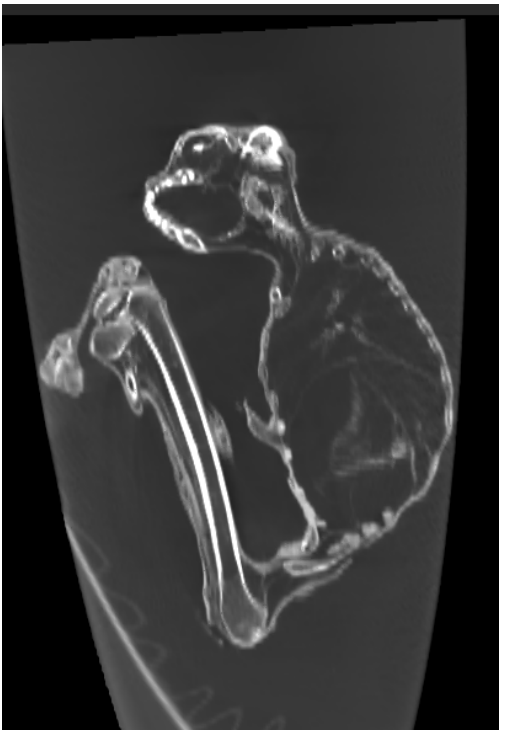

CT scans of the hip joints and femur.

Monserrat

The bones of the pelvis and hip, along with their respective joints, exhibit a conventional arrangement. The structure of the bones is standard, with the cortical layer expressed in the tubular bones.

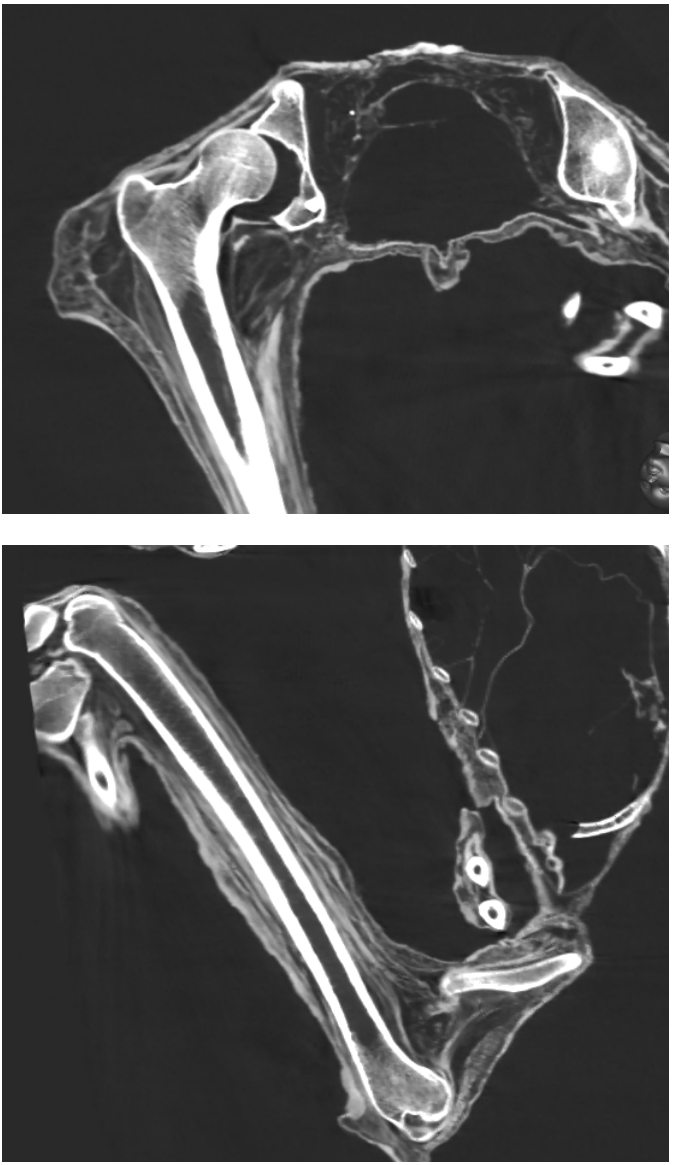

CT scans of the hip joints and femur.

Maria

The bones of the femur and tibia, their joints also have a classic configuration. The structure of the bones is standard, the cortical layer is expressed in the tubular bones.

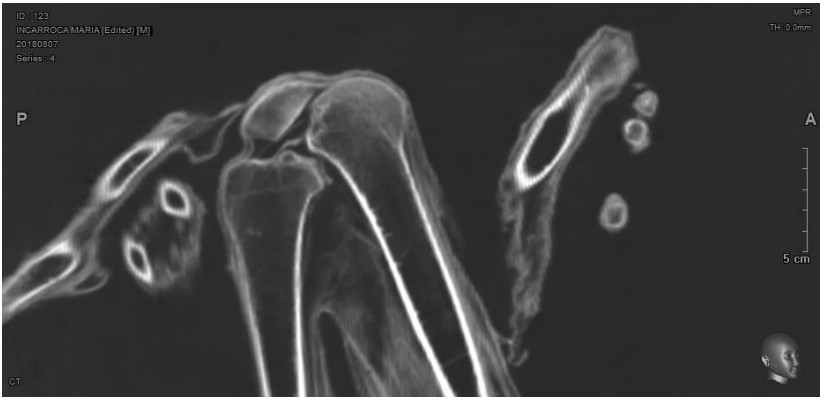

CT Screen knee joint

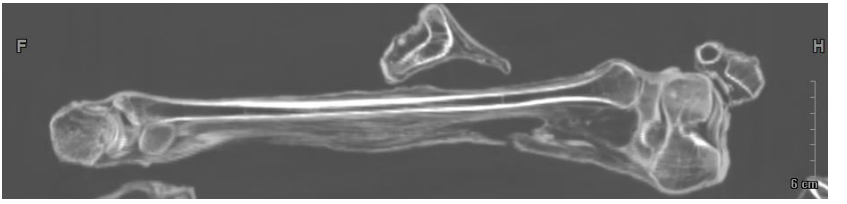

CT scan Left fibula

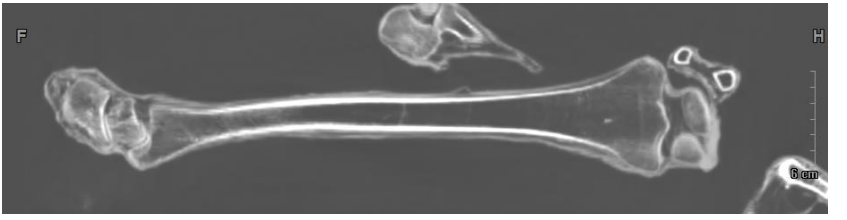

CT scan of the left tibia

The muscles of the calf and thigh are determined after dehydration without any damage to the integrity.

Monserrat

The following images depict a CT scan of the following body parts: the knee joint, the left fibula and tibia, and the ankle joint.

The muscles of the thigh and lower leg are characterised by their anatomical location and are in a state of dehydration. In the area of the knee and ankle joint, the congruence of the articular surfaces is preserved.

Hands

Maria

The carpal bones are of normal configuration and completeness (eight small bones), and there is no evidence of sesamoid bones. The metacarpal bones of non-human subjects are incomplete, with only three bones present. These bones exhibit a shape that is characteristic of humans. Absent or greatly reduced dorsal interosseous muscles and palmar interosseous muscles may indicate the absence of abduction and adduction movements of the fingers. During the post-processing stage of the analysis, the flexor and extensor tendons become clearly discernible.

Monserrat

The carpal bones are of normal configuration and completeness, comprising eight small bones. In contrast to the typical configuration observed in classical anatomy, the metacarpal bones exhibit an incomplete structure, comprising only three elements. These bones possess a distinctive morphology that is characteristic of the human species. The hand is constituted of three digits, each comprising three phalanges. The dorsal interosseous muscles and palmar interosseous muscles are either absent or significantly reduced, which may suggest a deficiency in the ability to abduct and adduct the fingers. During the post-processing phase of the hand, the flexor and extensor tendons become clearly discernible.

Reconstruction of the right hand. There is a foreign body, presumably metal, in the wrist area.

Maria

Post-processing – reconstruction of the right hand.

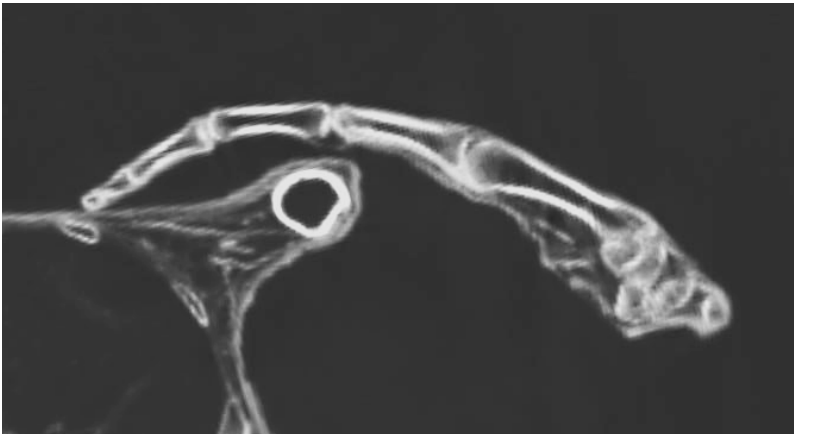

CT screen. Sagittal plane of the medial finger of the right hand.

When examining the distal phalanges, it seems that they consist of two parts - there is a bony bridge, but no full-fledged joint can be traced between them.

Monserrat

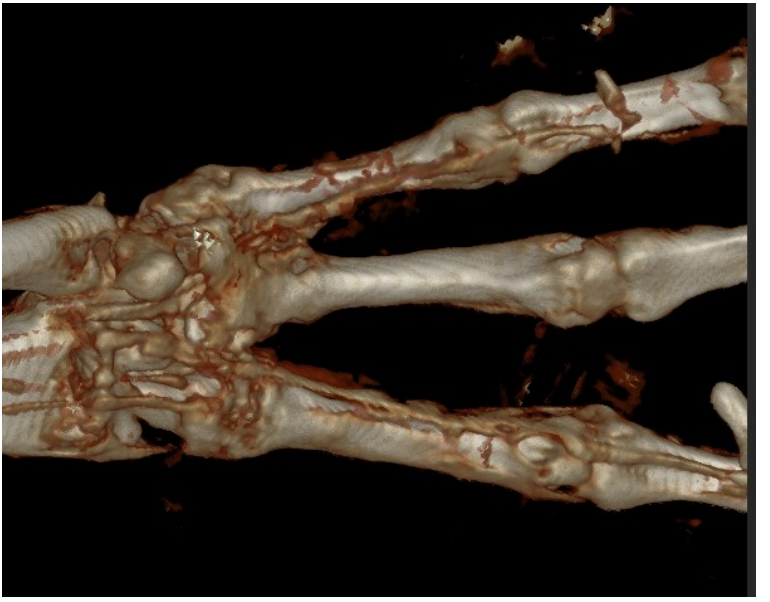

Reconstruction of the right hand. Palmar side.
Post-processing clearly shows tendon strands (flexors?).

Maria

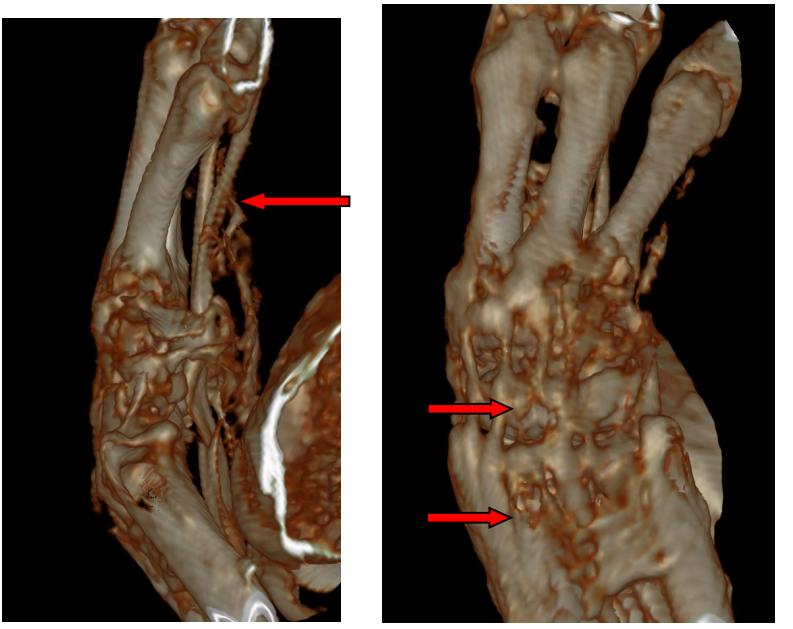

a b

Post-processing – reconstruction of the flexor (a) and extensor (b) tendons of the left hand.

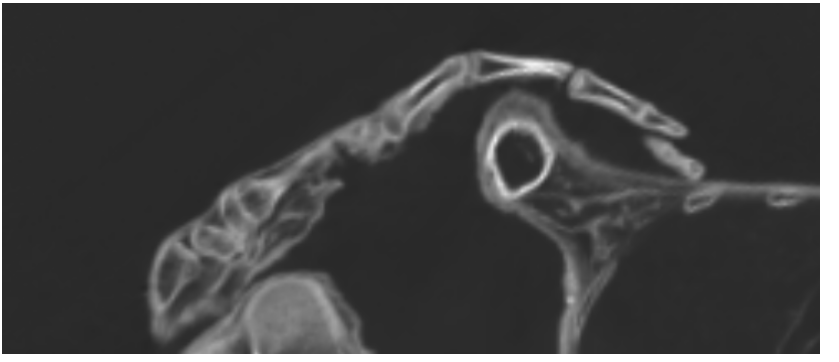

CT screen sagittal plane. Middle finger of the right hand.

Monserrat

Post-processing - reconstruction of the right hand. Wrist and metacarpal bones.

Post-processing – reconstruction of the right hand. Finger flexors are marked with arrows. No flexor reconstruction was obtained on the middle finger.

Monserrat

CT reconstruction of the left hand, back side.

Right hand, palm side.

Monserrat

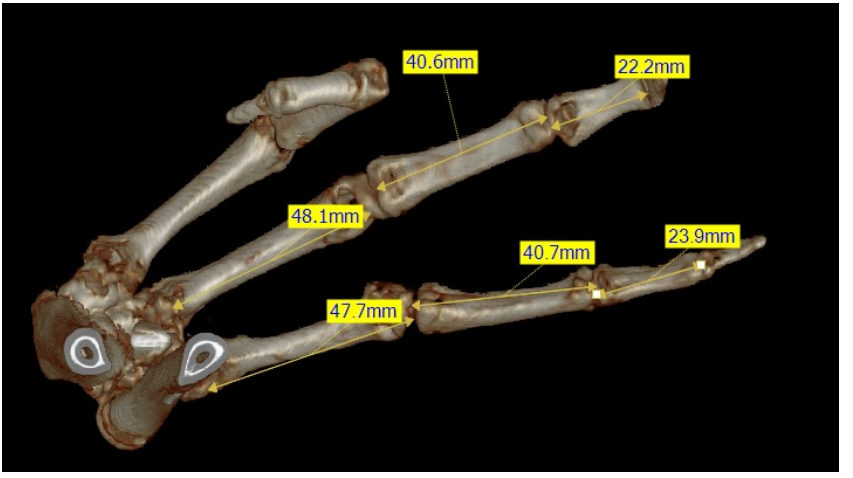

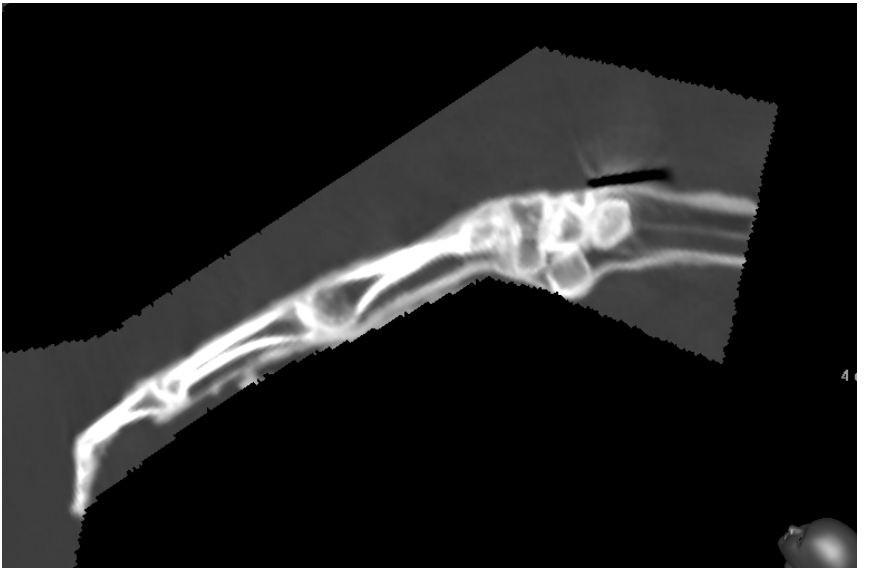

CT screen sagittal plane. Right hand middle finger.

Maria

CT scan of the wrist and metacarpus area.

Monserrat

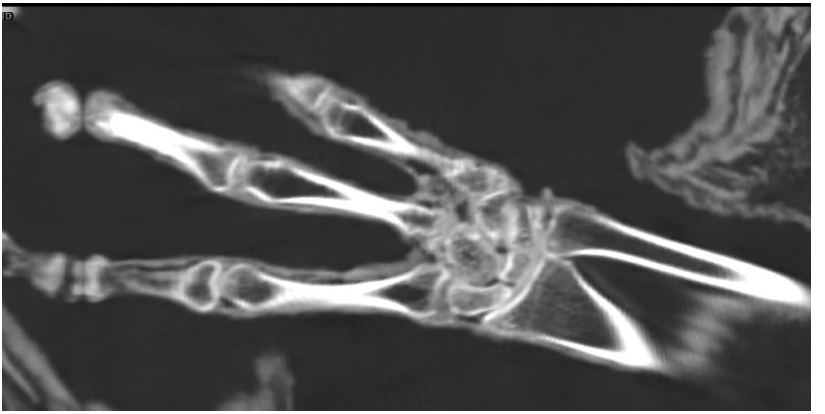

Right hand

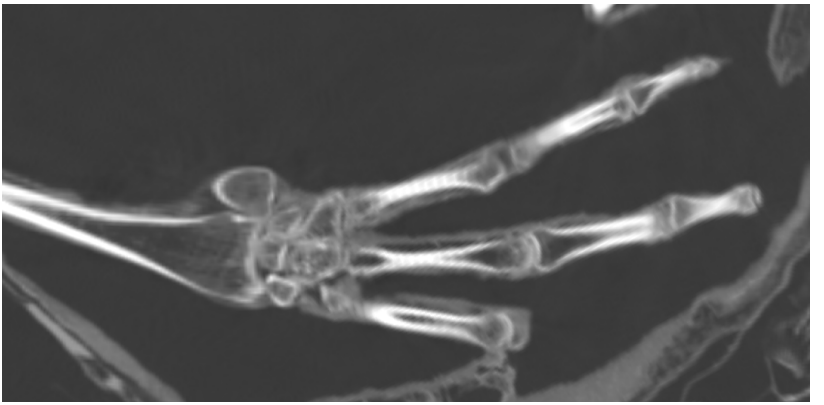

Left hand

Feet

Maria

Upon examining the feet, clubfoot is visible, especially on the left foot.

Monserrat

Upon examination of the right foot, the flexor tendons of the digits are observable, extending along the entire plantar surface and projecting to the toes. No traces of bone removal were detected.

Post-processing of the reconstruction of the right foot. Plantar surface.

Maria

The absence of a pronounced calcaneal tubercle.

The tarsal bones displayed normal configuration and completeness, with a total of seven bones observed. The presence of sesamoid bones was not detected. During the post-processing stage of the foot, the flexor and extensor tendons become visible, in addition to the calcaneal tendon (Achilles), which is intertwined with the reduced calcaneal tubercle.

CT screen sagittal plane and post-processing of foot reconstruction.

Monserrat

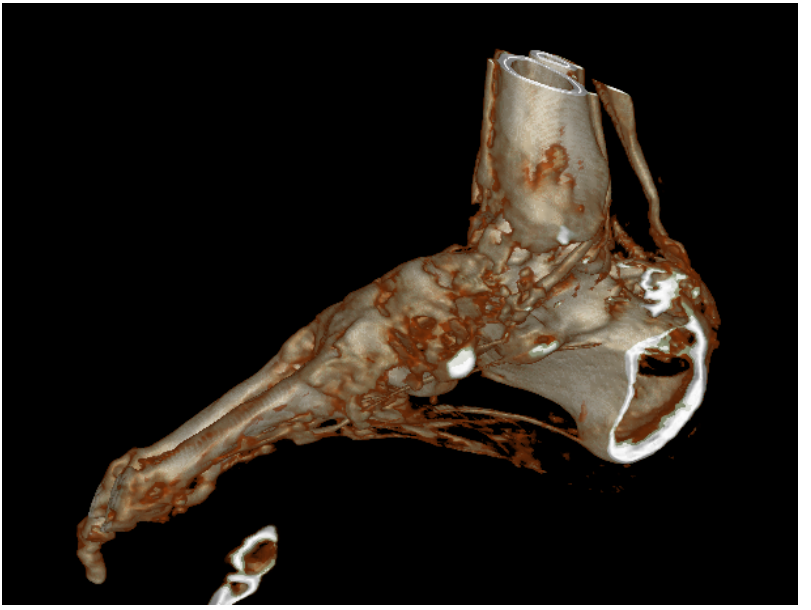

The following is a detailed report on the post-processing of the reconstruction of the right foot.

In contrast to the human foot, the metatarsus is comprised of only three bones. The foot is composed of three digits, each of which is endowed with three phalanges. No indications of forced removal of the metacarpal, metatarsal bones and phalanges of the fingers were observed.

Maria

Achilles tendon

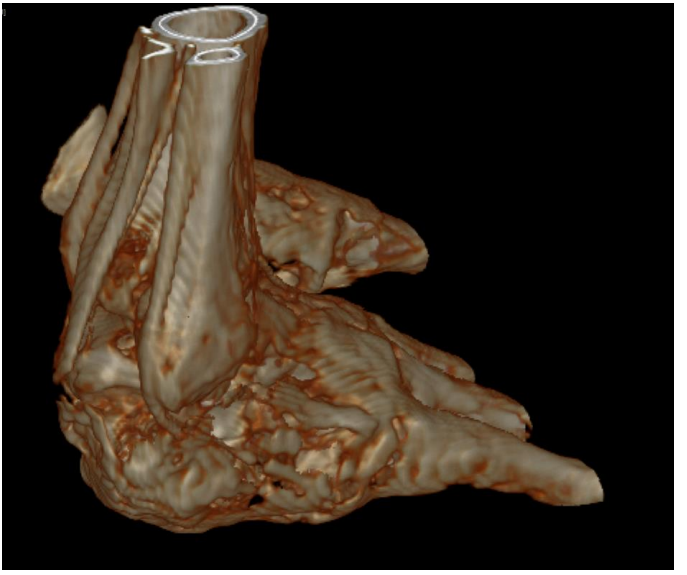

Peroneus longus tendon

Monserrat

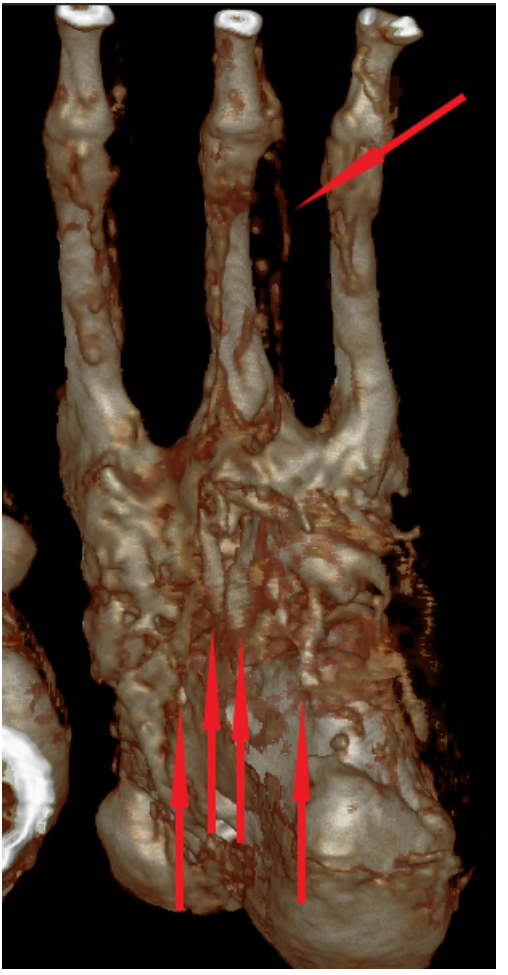

Maria

In contrast to the human metatarsus, which consists of a combination of three bones, the horse's metatarsus is composed of a single bone.

The foot is composed of three digits, each of which is endowed with three phalanges. There is no indication of any forced removal of the metacarpal, metatarsal bones, or phalanges of the toes.

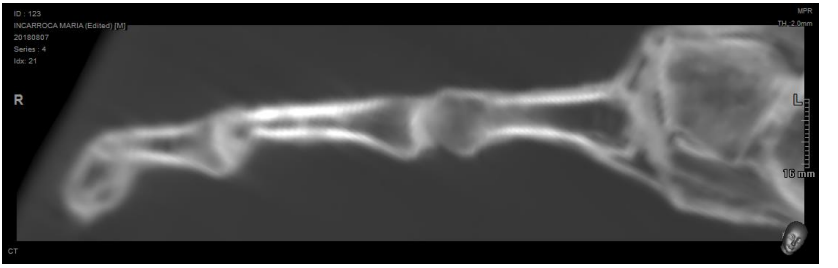

Phalanges of the fingers and metatarsus of the left foot.

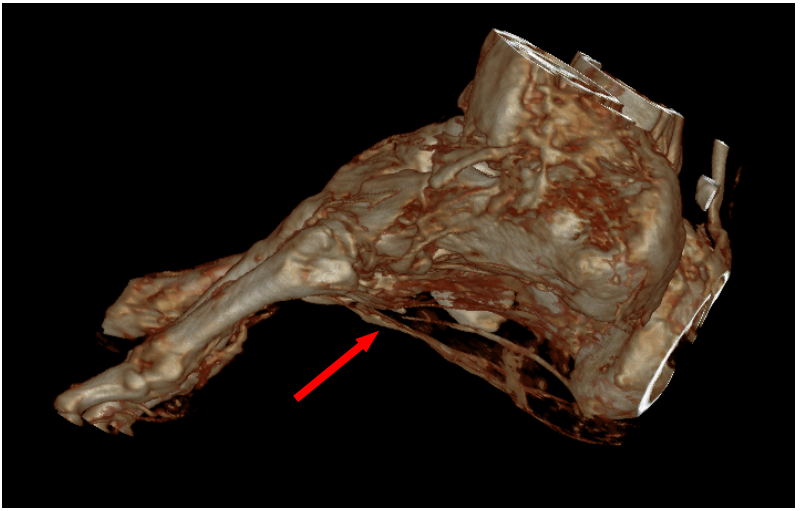

Reconstruction with post-processing of the left foot, view from below. Arrows indicate the flexor tendons of the fingers. Lateral surface of the foot.

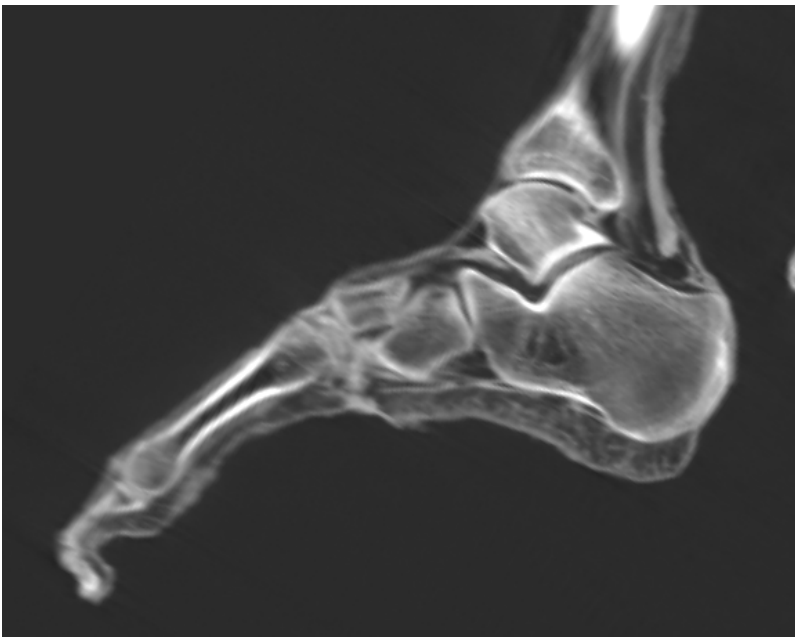

CT scan of the left foot, middle toe. sagittal plane.

Monserrat

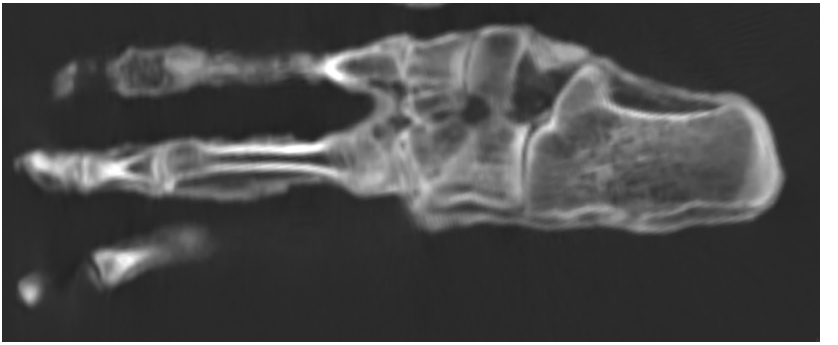

CT scans of the foot were performed in both the sagittal and horizontal orientations. The tarsal bones displayed normal configuration and completeness, with a total of seven bones observed. The presence of sesamoid bones was not detected.

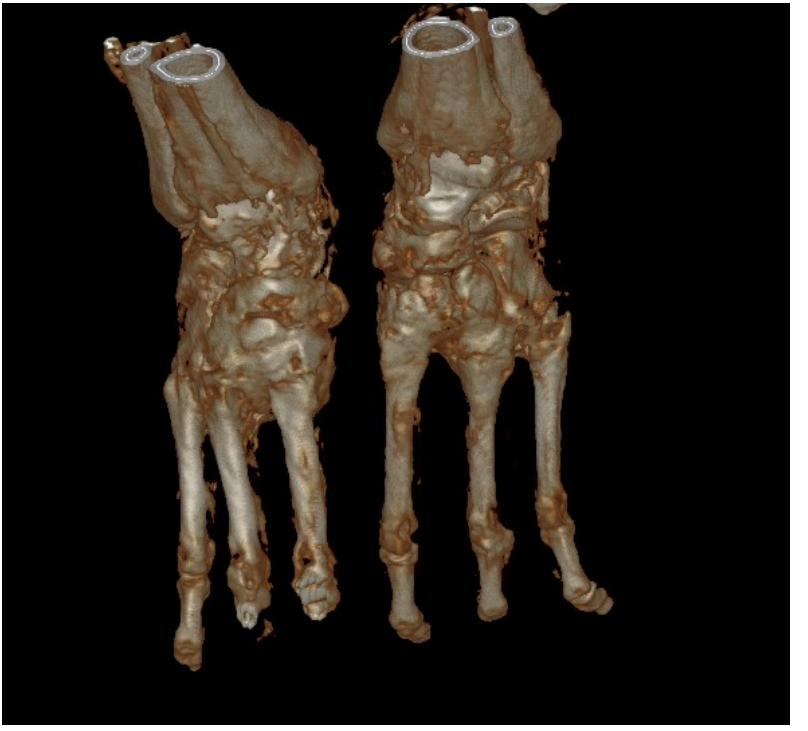

Feet reconstruction by post-processing. It is not possible to obtain an accurate image of the articulation of the tarsal bones - there is tissue compaction in the projection of the joints.

Monserrat

During post-processing of the foot, the flexor and extensor tendons are visible, as well as the Achilles tendon, which is woven into the calcaneal tuberosity.

Monserrat

Monserrat

Montserrat Pregnancy

When Montserrat died, she was pregnant - there was a child inside her.

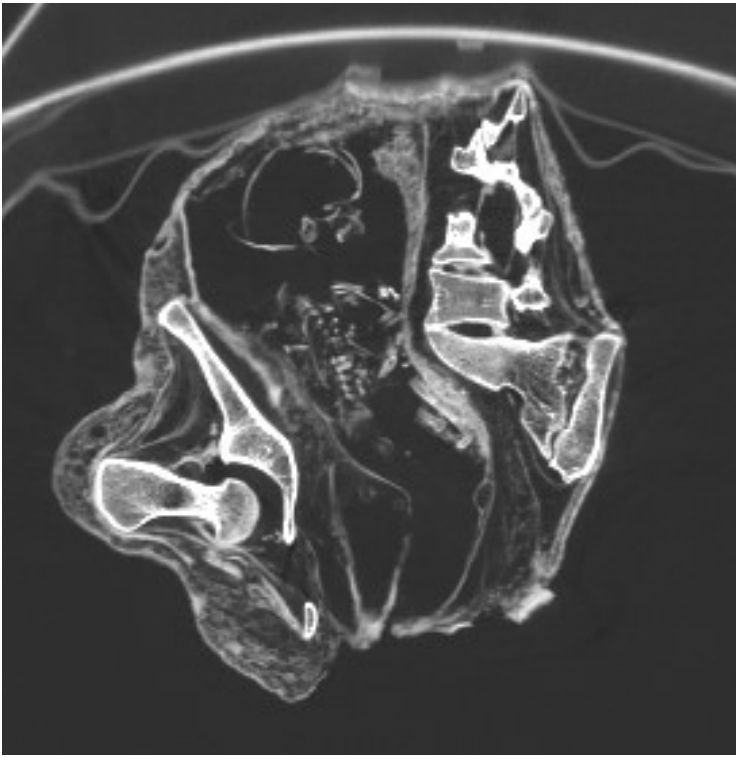

CT scans were performed in the oblique frontal plane. The position of the fetal head is determined by the displacement of the skull bones, ribs and vertebral bodies.

The length of the femur, which is 43 mm in this case, can be used to estimate the age of the foetus, which in this instance is approximately 30 weeks. The foetus is in a foetal position, i.e. the child lies with its feet down in the pelvic cavity.

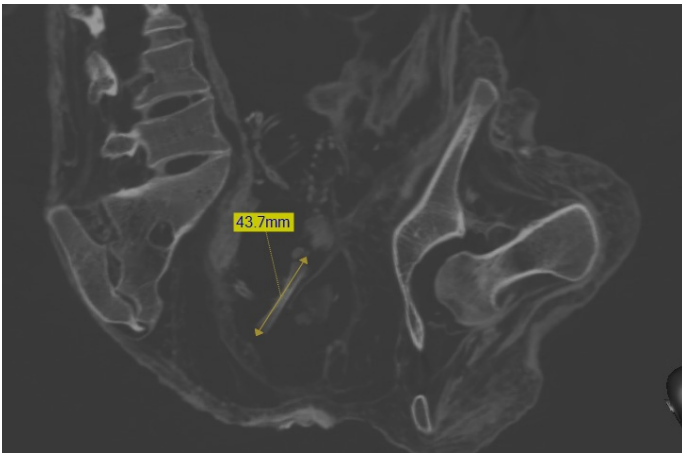

The measurement of the length of the fetal femur is of particular significance in this study.

The foetus is located within the uterus. During the process of dehydration of the uterus, the muscle tissue undergoes a reduction in size whilst retaining its shape.

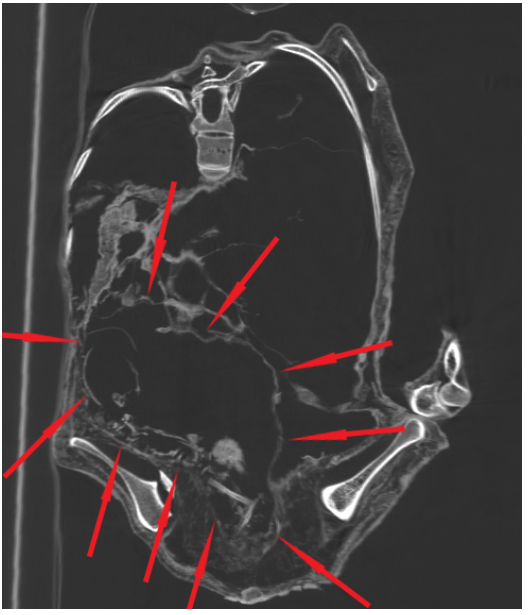

CT screen, frontal plane. Uterine borders are shown by arrows.

As a consequence of dehydration and the absence of stable bone suture formation, there has been significant displacement of the bones of the brain and facial regions. This is evident during fetal reconstruction, where the face is observed to be turned back. The foetus is positioned supine. The cranium is positioned at the level of the abdominal cavity, while the thoracic section and limbs are located at the level of the small pelvis. At this stage, the process of bone mineralisation is at an early stage. Consequently, an interruption in the image is evident in the area of the spinous processes and vertebral arches, with displacement of the ribs also observed. No images of the bone epiphyses are available.

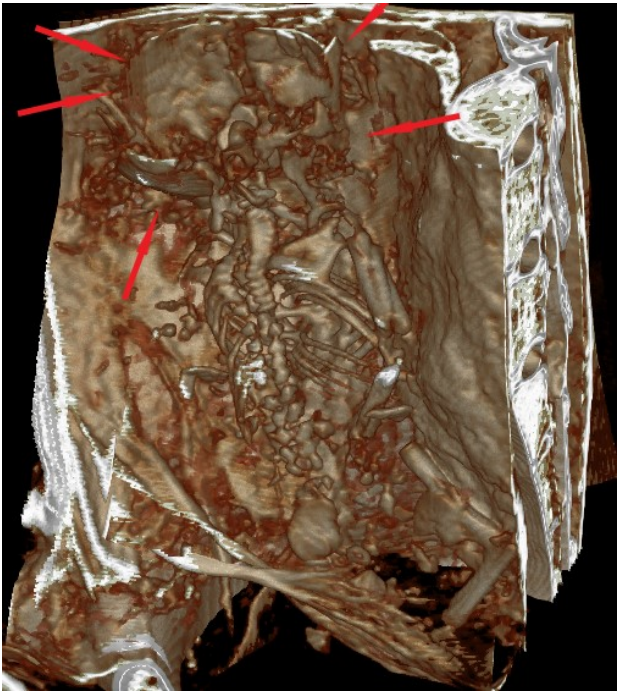

Reconstruction of the foetus, post-processing. The contour of the head is indicated by arrows.

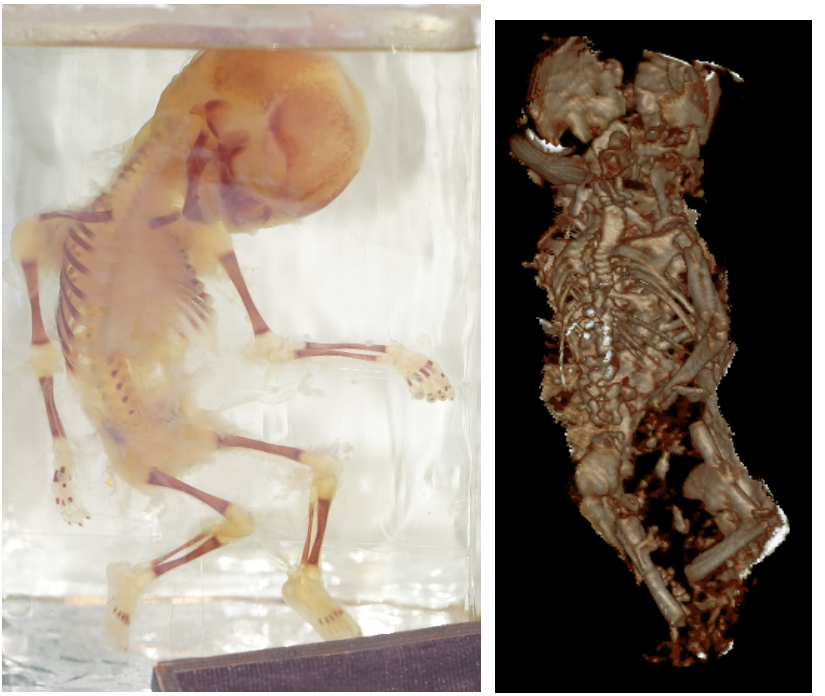

a b

a - In order to comprehend the image, a preparation is presented with tissue illumination and staining of mineralised bones (method of A.K. Kosourov and I.S. Gilbo). This method renders incomplete mineralisation of bones visible. b - Reconstruction of the foetus.

The reconstruction of the foetus. The head outline is indicated in red. The body outline is represented by the colour purple. The right scapula is visible in the shoulder region. The right humerus and ulna of the left arm, the femur and tibia of the left leg (bent) are visible and are shown in green. The spinal column is delineated in yellow. The greater wing of the left pelvic bone is indicated in blue.

Montserrat tissue density assessment using the Hounsfield scale.

A comprehensive evaluation of diverse tissues has been conducted, with the objective of generating a comprehensive database of constants for various tissues under conditions of dehydration. The integration of our data with that of other researchers is anticipated to facilitate the creation of a comprehensive compendium of constants for various tissues under dehydration conditions. It is imperative to acknowledge that under these conditions, tissues may undergo substantial changes in their characteristics. The existing tables reflect constants only for normal tissues (devoid of dehydration).

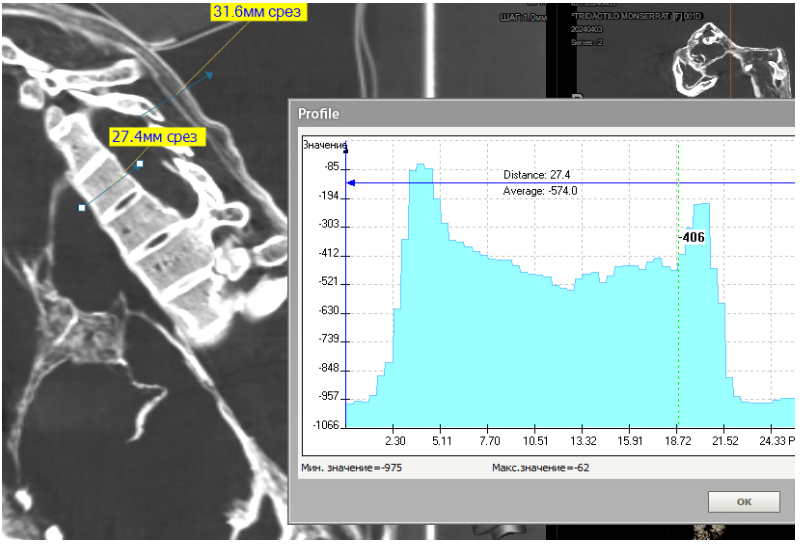

-62…- 200 HU. corresponds to the density of the cortical plate of the vertebral body. -400…-521 HU. corresponds to the density of the spongy substance of the vertebral body.

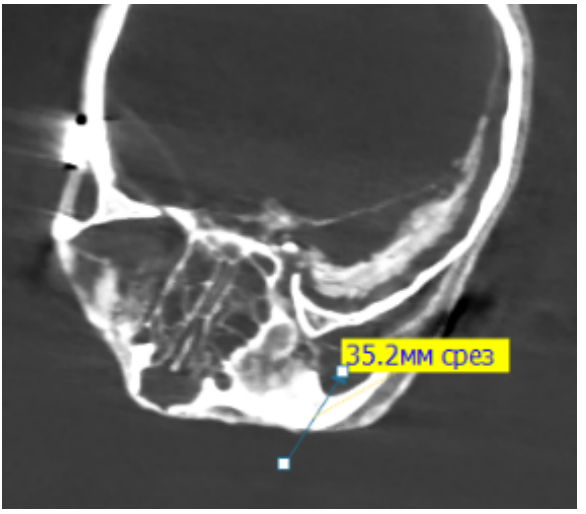

804…1745 HU. corresponds to the density of the zygomatic bone. The higher value corresponds to the anterior cortical plate.

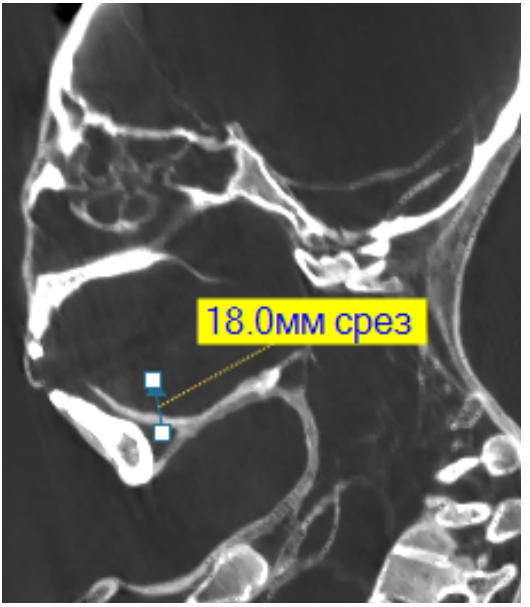

-209…- 510 HU. corresponds to the density of the tongue muscles.

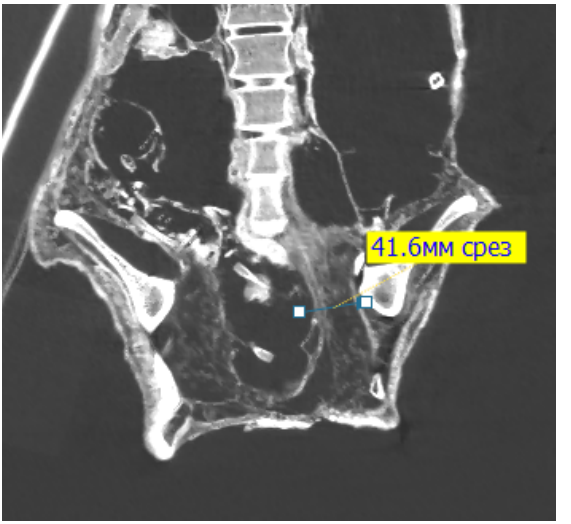

-800…- 821 HU. corresponds to the density of pelvic muscle tissue.

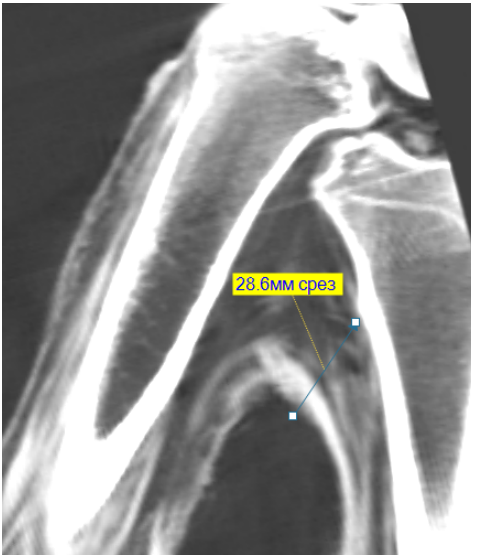

-680…- 770 HU. corresponds to the density of the calf muscle tissue.

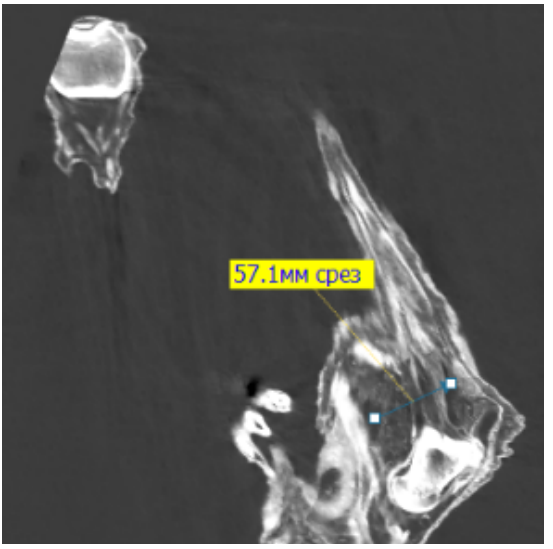

-755…- 890 HU. corresponds to the density of the thigh muscle tissue with tendon.

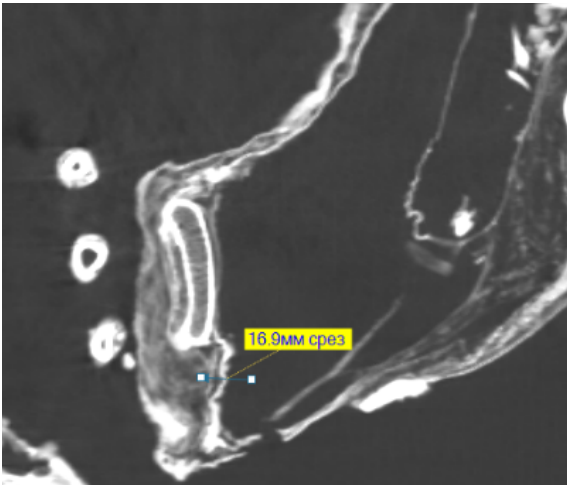

-470…- 630 HU. corresponds to the density of the bladder tissue. Moreover, the value of -470 corresponds to the bladder tissue with the peritoneum.

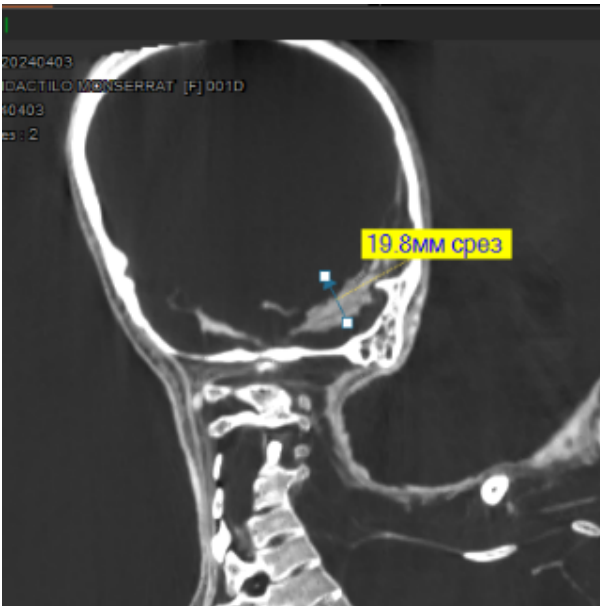

-466…- 550 HU. corresponds to the density of brain tissue.

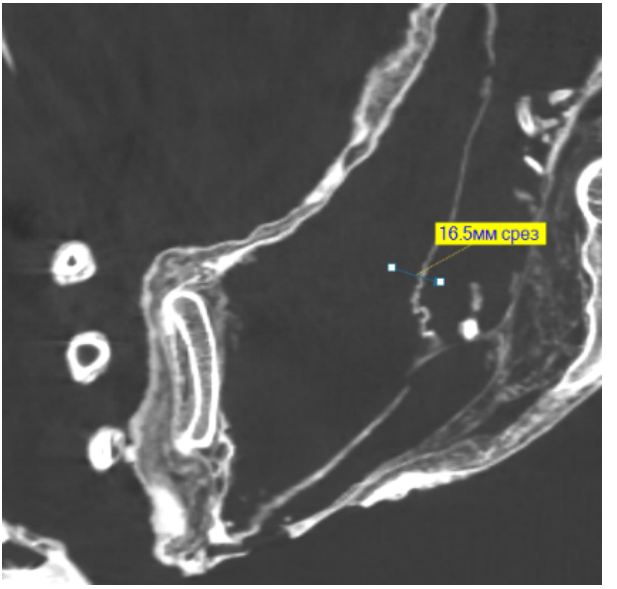

-666…- 829 HU. corresponds to the density of the uterine muscles.

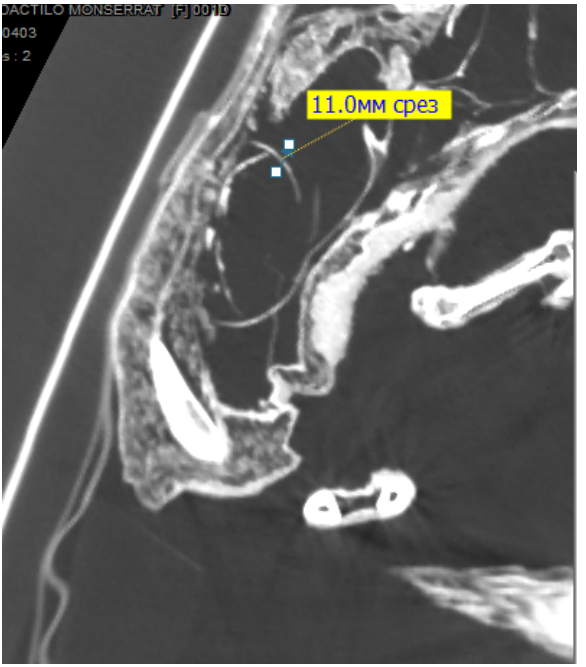

-700…- 770 HU. corresponds to the density of the fetal frontal bone.

-484…- 628 HU. corresponds to the density of the skin tissue of the back.

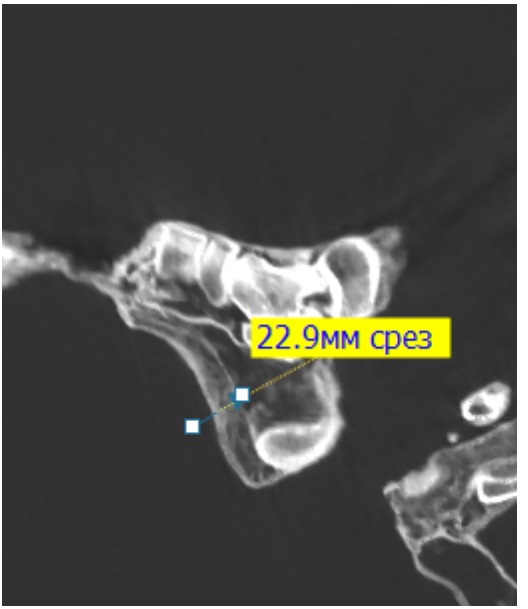

-540…- 405 HU. corresponds to the density of the heel skin.

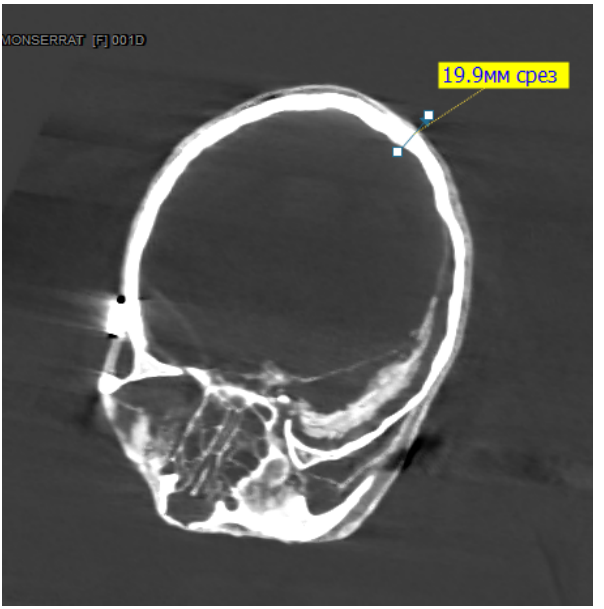

540…1194 HU. corresponds to the density of the occipital bone.

110

-600…- 719 HU. corresponds to the density of the diaphragm muscles.

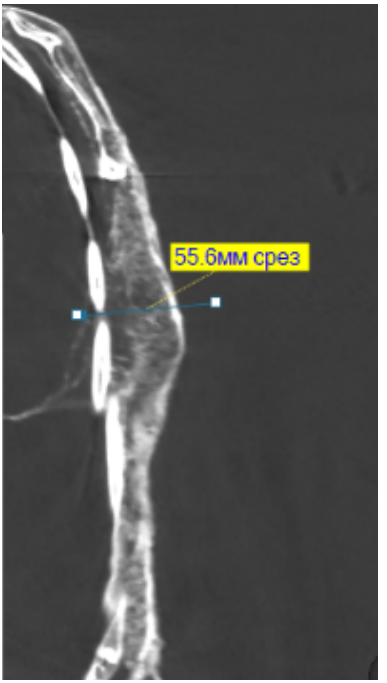

On average, -900 HU corresponds to the density of tissue with a hematoma.

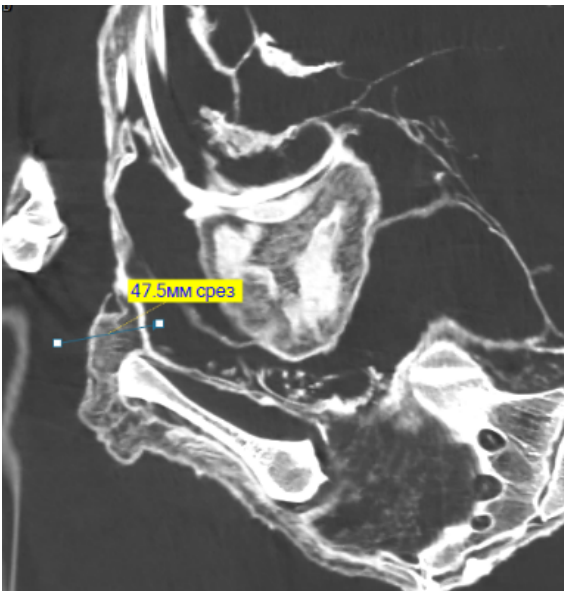

-700…- 878 HU. corresponds to the density of tissue with a hematoma in the iliac region on the right.

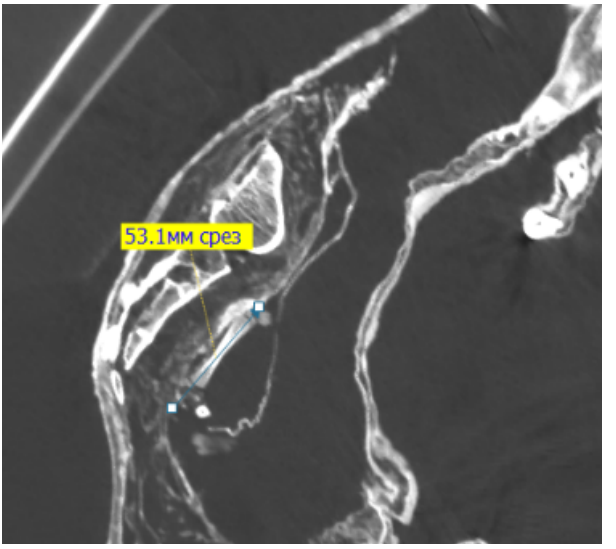

-50…- 438 HU. corresponds to the density of the fetal femur in the diaphysis zone, -540…-600 in the epiphysis zone.

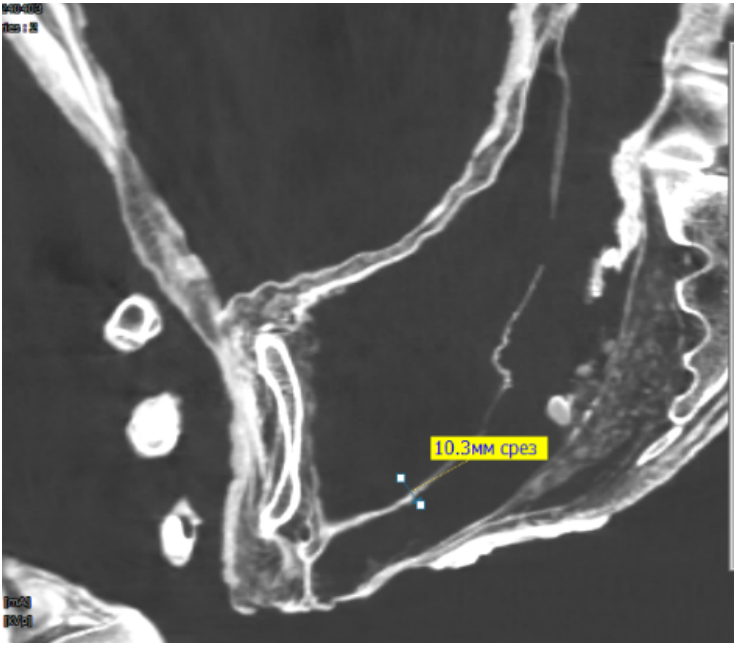

-369…- 930 HU. corresponds to the density of the colon wall.

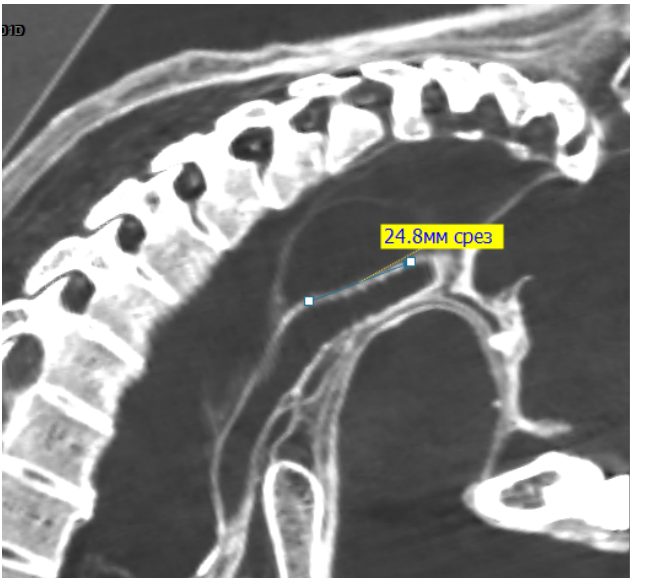

-657…- 700 HU. corresponds to the density of the trachea.

-560…- 970 HU. corresponds to the density of heart tissue.

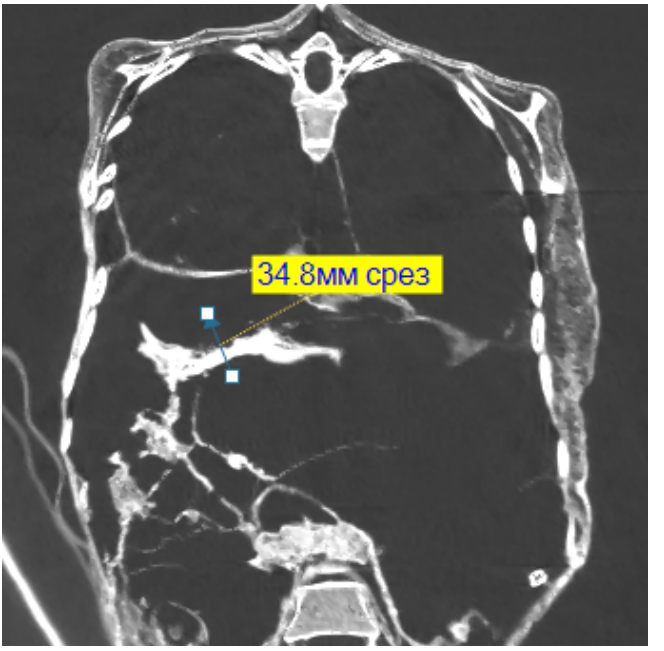

0…- 215 HU. corresponds to the density of liver tissue.

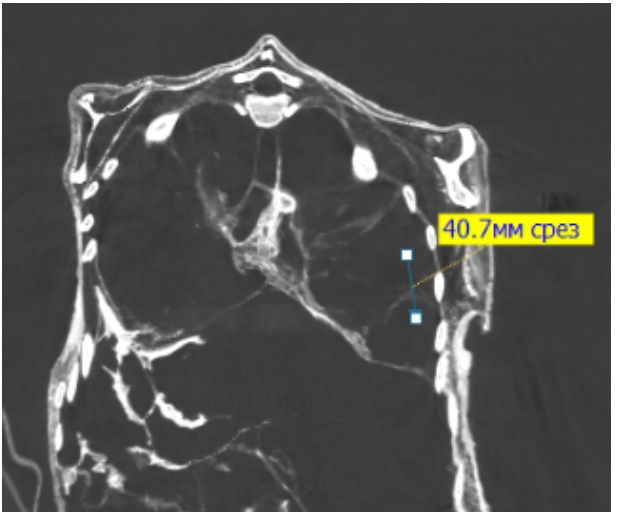

-919…- 935 HU. corresponds to the density of lung tissue.

skin and subcutaneous fat of the back	-484…- 628
skin and subcutaneous fat of the heel	-540…- 405
edema and hematoma in the chest area	793 …-900
edema and hematoma in the iliac region on the right	-700…- 878
cortical plate of the vertebral body	-62…- 200
spongy substance of the vertebral body	-400…-521
zygomatic bone (cortical plate)	804…1745
occipital bone (cortical plate)	540…1194
foetal frontal bone	-700…- 770
foetal femur in the diaphysis area	-50…- 438
foetal femur in the epiphysis area	-540…-600
tongue muscles	-209…- 510
diaphragm muscles	-650…- 719
pelvic muscles	-800…- 821
calf muscles	-680…- 770
thigh muscle with tendon	-755…- 890
brain tissue	-466…- 550
heart tissue	-560…- 970
trachea	-657…- 700
lung tissue	-919…- 935

liver tissue	0…- 215
uterine muscles	-666…- 829
bladder tissue	-470…- 630
colon walls	-369…- 930

Conclusions

The presented material provides unequivocal evidence that the mummies examined are indeed the original remains of real creatures that underwent natural mummification after death. It is evident that they are not dummies, nor are they a combination of parts of individual animals. Concurrently, online sources have been identified that purport to demonstrate the forgery of the mummies from the Nazca region. A thorough review of the extant literature reveals a conspicuous absence of any analysis of CT scans. Nevertheless, the possibility of forgery cannot be discounted, given the propensity of private collectors to allocate financial resources towards the acquisition of authentic artefacts. It can be stated that the CT scans under review were obtained by means of tomographic imaging of real individuals.

The process of natural mummification is a well-documented phenomenon in Mesoamerica. In the Mexican city of Guanajuato, the Museum of Mummies is home to a collection of 111 mummies, 59 of which are on display. These mummies were exhumed between the mid-19th century and 1958, a period during which a law was in effect requiring relatives to pay a tax so that the bodies of their loved ones could be kept in a cemetery. In the event of non-payment of the tax in a timely manner, the right of the relatives to the burial site was revoked, and the remains were removed from the stone tombs. It was subsequently established that a number of these individuals had undergone a natural mummification process, and that they were stored within a dedicated facility located within the cemetery grounds. Subsequent to this, the mummies were transferred to the museum, which opened to the public in 1969, and they were exhibited in glass cases. As stated on the official website, the museum receives hundreds of thousands of visitors on an annual basis.

The phenomenon of natural mummification is attributable to elevated temperatures during the day and a dry climate. The Nazca region, situated in the southernmost reaches of Peru, is distinguished by an arid climate. In this region, rainfall is very rare, with an annual precipitation of less than 25 mm. For the majority

of the year, the region experiences arid and sun-drenched weather, thus classifying it as one of the driest places on Earth. This phenomenon can be attributed to the cold Humboldt Current, which exerts a cooling effect on the atmosphere, thereby hindering the development of cloud formations and precipitation. Consequently, the discovery of mummies in the mountain caves of the Nazca region is not unexpected. The anatomical features of these mummies indicate that we are faced with an anomalous phenomenon that requires careful study. Concurrently, it is regrettable that despite the substantial number of studies conducted on these mummies by scientific groups in various countries, the results of radiocarbon and genetic analysis are being deliberately disregarded by official science. While the results were reported at a conference in the Peruvian Congress in 2018, a number of papers have been published on the study of these mummies.

In 2018, Dr. Linda Moulton Howe from London published a detailed analysis of the structural features of the mummy of Maria (https://www.earthfiles.com/2018/05/30/part-1-latest-genetech-dna-results-on-3-fingered-bodies-from-palpa-nazca-region-of-peru/). Professor Konstantin Korotkov published a book in 2019, entitled "The Mysterious Mummies of Nazca", which was released in Russian, English and Spanish. A group of authors from the Laboratory of Health of Mexico and the University of Limassol, Cyprus, published a paper in which the skulls of mummies were compared with the skull of a llama, and a fundamental difference in their structure was shown (José De La Cruz Ríos López, Georgios A. Florides, Paul Christodoulides. The application of CT-scanning for the identification of a skull from an archaeological find of unknown origin in Peru. International Journal of Biology and Biomedicine. 6. 46-65. 2021). An analysis of Maria's CT scans is presented in the work of a group of authors from Peru and Mexico (Edgar Hernández-Huaripaucar, Roger Zúñiga-Avilés, Bladimir Becerra-Canales, Carlos Suarez-Canlla, Daniel Mendoza Vizarreta, Irvin Zúñiga-Almora). This paper sets out to explore the morphological and anatomical biometry of the antediluvian human-like tridactyl specimen from Nasca-Peru. The Revista de Gestão Social e Ambiental (RGSA) is a publication that was first established in 2024. The Digital Object Identifier (DOI) for this article is: https://doi.org/10.24857/rgsa.v18n5-137. The conclusion drawn from this analysis is that the mummies under

scrutiny are not mere artefacts, but represent real creatures. In his 2024 book Expediente abierto, the Mexican author Martín Achirica Ramos presented a comprehensive overview of the extant data concerning the Nazca mummies at that time.

Presently, researchers in Peru possess six mummies that bear a resemblance to Maria and Montserrat. This finding suggests the hypothesis that these creatures may represent a distinct species of Homo sapiens, termed Homo sapiens Nazca, although this remains a subject of further research. In any event, it is evident that the artefacts in question are of significant interest and require further consideration and research.

The potential for the analysis of CT scans of two specimens of creatures exhibiting comparable abnormal characteristics – namely, elongated skulls and distinct features, in addition to three fingers on their hands and feet – suggests the possibility that they may represent a distinct type of humanoid creatures, divergent from Homo sapiens sapiens. It is to be hoped that in the future further specimens of such creatures will be presented for research.

It is hoped that the material presented will be utilised by interested specialists and enthusiasts for a more detailed understanding of this unique phenomenon.